

790

No



NATIONAL AERONAUTICS AND SPACE ADMINISTRATION

INTERNAL NOTE MSC - EG - 69 - 21

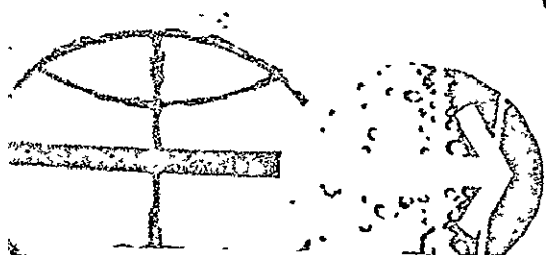
PROJECT APOLLO

STABILITY ANALYSIS OF APOLLO ATTITUDE CONTROL
DURING SERVICE PROPULSION THRUSTING

SYSTEMS ANALYSIS BRANCH
GUIDANCE AND CONTROL DIVISION

MANNED SPACECRAFT CENTER
HOUSTON, TEXAS

March 5, 1969



N70-34737

(ACCESSION NUMBER)

72

(PAGES)

TMX-64413

(NASA CR OR TMX OR AD NUMBER)

(THRU)

(CODE)

21

(CATEGORY)

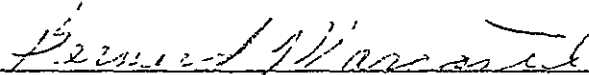
Reproduced by
NATIONAL TECHNICAL
INFORMATION SERVICE
Springfield, Va 22151

FACILITY FORM 602

PROJECT APOLLO

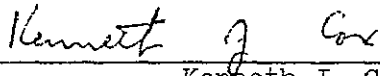
STABILITY ANALYSIS OF APOLLO ATTITUDE CONTROL
DURING SERVICE PROPULSION THRUSTING

PREPARED BY



Bernard Marcantel

APPROVED BY



Kenneth J. Cox

Chief, Systems Analysis Branch



Donald C. Cheatham

Assistant Chief, Guidance and Control Division



Robert G. Chilton

Deputy Chief, Guidance and Control Division

NATIONAL AERONAUTICS AND SPACE ADMINISTRATION

MANNED SPACECRAFT CENTER

HOUSTON, TEXAS

MARCH 5, 1969

SUMMARY

Results of analysis for determination of the nominal stability margins, of the thrusting flight attitude control system, for the Apollo CSM spacecraft are given. The stability margins are presented for both the pitch and yaw control channels, using both the Primary Guidance and Navigation System Digital autopilots and the Stabilization Control System analog autopilots. Analyses were performed for the spacecraft in the docked and undocked configurations, and for various SPS propellant load conditions in each configuration.

INTRODUCTION

This stability analysis was performed for the Apollo CSM spacecraft autopilots used during Service Propulsion System (SPS) thrusting maneuvers. The autopilots used for this function are called the Thrust Vector Control Digital Autopilot (TVC DAP) and the Stabilization and Control System (SCS). Each autopilot system analyzed required separate forward loop compensation and gain constants for the CSM alone and the CSM/IM docked configurations. Figure 1 gives the general functional flow for the TVC DAP. The filters used with the TVC DAP were for the COLOSSUS I flight program. A general functional flow of the SCS autopilot is presented in figure 2.

The purpose of this analysis was to compute the nominal Apollo spacecraft stability margins using the bending data of reference 3. A detailed tabulation of all the data used in the analysis is presented for reference. A concentrated effort was made to combine this data correctly in the mathematical model being used for the detailed airframe dynamics, including all significant coupling between bending modes, sloshing propellant modes, and the SPS engine actuation servo. Spacecraft stability margins were computed for both the pitch and yaw channels, for the docked and undocked spacecraft configurations, and for various SPS propellant loads.

The general layout of this report is as follows. There is a short discussion of the spacecraft math model, with appropriate references to data used, followed by a description of the analysis techniques. This is followed by a detailed discussion of the analysis results and a statement of conclusions.

A similar analysis using more recent Apollo bending data and also presenting an analysis of the COLOSSUS II TVC DAP is documented in another internal note, reference 11.

Spacecraft Model

The spacecraft dynamical model was programmed on the CDC 3800 digital computer. The digital programs used in deriving the spacecraft transfer function were AIRFRAME and POLYMES. These programs are documented in reference 8. The equations of motion in program AIRFRAME are written for a single axis spacecraft model including equations for an engine mode, a rigid body mode, an actuator model, structural bending modes and slosh modes. The program AIRFRAME computes coefficients for the differential equations from pertinent input data. These coefficients are then input into the POLYMES program which solves for the S-plane transfer function. The transfer function is then inserted into a general control systems program for analysis. A description of the control systems program used in this analysis is given in reference 9. This program has the capability of performing Z-transforms, W-transforms, frequency responses, plotting, block diagram manipulations, and a limited amount of time domain analyses.

Input parameters used in the analysis for various fuel loadings and configurations are presented in Table I. Definitions of symbols in this table may be found in Table II. The data was the latest available at the time the analysis was performed.

Actuator, servo electronics, and engine data were obtained from reference 1. The airframe mass and inertia data were obtained directly or calculated from data in references 2 and 3. The latest available mass properties data were used. Due to the modeling of the airframe equations, masses of the sloshing propellant and the engine were input separately from the airframe. This removal causes shifting in the airframe center of gravity; therefore, data dependent on the c.g. location would be slightly different from the data presented in the references. This same procedure was true in simulating the airframe and engine inertia.

Sloshing propellants in the SPS storage and sump tanks were treated as linear spring mass systems. Sloshing in each tank is characterized by a slosh mass, a slosh frequency, and a slosh mass attach point which are functions of the tank geometry, fluid levels, and acceleration. Sloshing effects in the SPS sump tanks are negligible when there is fuel remaining in the storage tanks; therefore, sump tank sloshing was not simulated when using a CSM configuration with propellant in the storage tanks. Slosh damping ratios were assumed constant (.0007) for this analysis. The CSM sloshing data was obtained directly (or calculated when not available) using references 2 and 3. This data was derived from mechanical analogies of the fluid motions. The mechanical models were designed to produce the same forces and moments on the vehicle as the fluids produce during disturbances, and at the same frequencies at which the fluids respond.

LM propellant slosh data was determined from curves in reference 4. These curves were calculated from actual LM tank models and verified experimentally. The slosh masses for the LM ascent and descent tanks were also treated as linear spring mass systems in this stability analysis.

The CSM/LM dynamic characteristics are sufficiently different from those of the CSM alone to require the use of separate primary control system digital autopilot (DAP) filters for each configuration and separate backup, continuous data control system filters for each configuration. These four separate control system filters are described below. The digital filter used with the CSM/LM TV DAP is a seventh order filter of the form:

$$D(z) = K_z \frac{1 + N_1 z^{-1} + N_2 z^{-2} + N_3 z^{-3} + N_4 z^{-4} + N_5 z^{-5} + N_6 z^{-6} + N_7 z^{-7}}{1 + D_1 z^{-1} + D_2 z^{-2} + D_3 z^{-3} + D_4 z^{-4} + D_5 z^{-5} + D_6 z^{-6}}$$

The coefficient values are as follows:

$N_1 = -2.9708$	$D_1 = -4.7798977$
$N_2 = 3.1947$	$D_2 = 9.4452763$
$N_3 = -0.4096$	$D_3 = -9.8593475$
$N_4 = -2.5780$	$D_4 = 5.7231811$
$N_5 = 2.9629$	$D_5 = -1.7484250$
$N_6 = -1.5101$	$D_6 = 0.21933335$
$N_7 = 0.3124$	

This filter is for the COLOSSUS I DAP of reference 5, low bandwidth mode. This mode has a sampling frequency of 12.5 samples per second and is initiated six seconds after thrust initiation. The gain factor associated with the filter varies in inverse proportion to the vehicle gain TL_x/I , so that a constant frequency bandwidth can be maintained during a burn. For this filter, the gain relationship was $K_z (TL_x/IAVG) = 1.80 \times 10^{-3} \text{ 1/sec}^2$.

T - thrust of vehicle, lbs.

l_x - distance from engine gimbal point to vehicle c.g., ft

IAVG - average spacecraft pitch and yaw moment of inertia, slug-ft².

The values of K_z used for the various fuel loadings may be found in Table I.

The CSM alone DAP filter is a third order filter of the following form:

$$D(z) = K_z \left[\frac{N_0 + N_1 z^{-1} + N_2 z^{-2} + N_3 z^{-3}}{D_0 + D_1 z^{-1} + D_2 z^{-2} + D_3 z^{-3}} \right]$$

The coefficient values are as follows:

$$\begin{array}{ll} N_0 = 1.0 & D_0 = 1.0 \\ N_1 = -1.480247 & D_1 = -2.062524 \\ N_2 = 0.553559 & D_2 = 1.565661 \\ N_3 = -0.057085 & D_3 = -0.401160 \end{array}$$

This filter has been defined in reference 6. A sampling frequency of 25 samples per second was used with the following gain factor, $K_z(Tl_x/IAVG) = 8.4$. Calculated values of K_z for various fuel loadings may be found in Table I.

The forward loop cascade compensation for the CSM/IM autopilot of the backup control system is as follows:

$$\left[\frac{\left(\frac{s}{8.17}\right)^2 + \frac{2(0.043)s}{8.17} + 1}{\left(\frac{s}{9.39}\right)^2 + \frac{2(4.72)s}{9.39} + 1} \right] \left[\frac{\frac{s}{8.38} + 1}{\frac{s}{8.41} + 1} \right] \left[\frac{1}{\frac{s^2}{80} + \frac{2(0.5)s}{80} + 1} \right]$$

This filter was given in reference 7. Feedback loop configuration and gains are defined in figure 2. The forward loop compensation for the CSM alone configuration was given in reference 1 and is defined as follows (see figure 2 for loop gains):

$$\frac{1}{\frac{s}{40}^2 + \frac{2.0s}{40} + 1} .$$

Analysis Techniques

The frequency response method of analysis was used in determining the stability margins of the various spacecraft configurations. The essential feature of the frequency response method is to determine amplitude and phase shift of the control variable that is produced for assumed unit amplitude sinusoidal forcing functions, for all frequencies. When the feedback is in phase with the forcing function, with an amplitude of unity or greater, the system is unstable.

The sinusoidal transfer function, written in terms of the Laplace operator, s , is a complex function of the complex variable s , and its response can be represented by a magnitude and phase angle (Bode plots). The same data can also be displayed on one plot by plotting amplitude versus phase, which is the method chosen in this analysis. These curves are a plot of the magnitude in decibels versus phase shift, on rectangular coordinates, with frequency as a varying parameter on the curve. The choice of this data format provides ease in determining stability margins explicitly from the data plots and clearly defines amplitude and phase relationships of the slosh and bending resonances.

Stability characteristics of a system may be specified in terms of gain margins and phase margins. Gain margin is the amount by which the gain of a particular branch may be allowed to increase before producing instability. Using figure 5 as an example, the gain margin is determined from the plot by the gain increase in decibels (5.8 db) required to produce unity amplitude (zero db), for the frequency where the phase angle is 180 degrees (180 instead of zero because there is phase reversal by the controller). The crossover point must occur below the 0 db coordinate for the system to be stable.

Phase margin is the amount of phase shift that would produce instability at the frequency where the curve crosses the 0 db coordinate. Again, using figure 5 as an example, the phase margin would be the angle (41.3 degrees) between the (0 db, 180°) point and the curve intersection of the 0 db coordinate. This condition derives from the fact that the planar airframe transfer functions under study here have two free roots at the origin but no poles in the right half plane. Nyquist stability criteria dictates that the frequency response plots should pass to the right of the 180 degree line when amplitude is passing through unity.

In the CSM/LM transfer function, each significant bending and slosh mode results in a complex pole-pair that is immediately preceded by a complex zero-pair. This same zero-before-pole configuration occurs in the CSM alone except for the full case, which is discussed further in the discussion section of this report. Each pole-zero pair produces a closed contour in the gain-phase which must be prevented from encircling the 0 db, 180° point. In the Apollo CSM spacecraft, all the zero-pole pairs of slosh and bending occur at frequencies above the main crossover frequency; therefore, any potential encirclement of the 0 db, 180° point would have to be the result of the resonance peaks produced by the airframe or actuator dynamics. The resonance peaks may be prevented from reaching the 0 db line by attenuation in the autopilot filter, or they may be "phase compensated" to prevent resonant peaks that are greater than 0 db from encircling the 0 db, 180° point. Both of these approaches were used by the designers of the Apollo spacecraft autopilots. These techniques are referred to as gain stabilization and phase stabilization respectfully.

Control of the spacecraft with the primary control system involves the use of a sampled-data system. The frequency response methods just described were developed for continuous systems; therefore, approximations would have to be made or some other techniques applied for analysis of sampled-data system. All significant poles and zeros of the spacecraft configurations studied occurred at frequencies that were well below half the sampling frequency of the digital autopilots; therefore, as a first order approximation it would have been possible to treat the digital autopilot dynamics as if it were a continuous system. The gain-phase frequency response analysis in the S-plane could then have been applied. Another approach is the conversion of the continuous plant transfer function into a pulse transfer function and then transforming to a complex variable domain where continuous-data system analysis methods could be applied. The mapping of a sampled-data system transfer function into the W-plane is a method using this approach. Sampled-data systems, normally described in the Z-plane, may be mapped into the W-plane by the bilinear transformation;

$Z = \frac{1 + W}{1 - W}$. This maps the unit circle of the Z-plane into the entire

left half of the W-plane and the characteristic polynomials in Z are then converted into polynomials in W of the same order. This approach produces a frequency response curve for the pseudo frequency, $\text{Im}(W)$, that is shaped exactly like the S-plane version, at frequencies well below the sampling frequency, unless frequency folding effects were predominant. This technique has the advantage of being exact, and so the W domain approach was used for this analysis.

The reader is referred to reference 10 for a complete development and discussion of the analysis techniques discussed only briefly above. One final comment is that real frequency (ω) is related to the pseudo frequency, $\text{Im}W$, by the following relationship:

$$\text{Im}W = v = \tan \frac{\omega T}{2}, \text{ where } T = \text{sample period.}$$

Similarity of the gain-phase plots in the S and W planes for the spacecraft dynamics transfer function are shown in figures 3 and 4 respectively. The two curves are almost identical except for the additional phase lag that is evident in the W-plane curve. This phase lag is more pronounced at the higher frequencies. Also, if any significant frequency folding effects had been present, the curve shapes would be different at the lower frequencies.

The continuous transfer function used to derive the S-plane gain-phase plot of figure 3 is given in the root format as follows:

<u>Zeros</u>		<u>Poles</u>	
<u>Real Roots</u>		<u>Real Roots</u>	
-5.00000000+01		-1.95434341+01	
<u>Complex Roots</u>		<u>Complex Roots</u>	
σ	ω	σ	ω
9.17752-03	2.377714+01	-2.685049+01	9.785229+01
-3.003204-02	8.762565+00	-6.626550-02	1.418702+01
-1.931401-03	2.753396+00	-2.447407-03	3.453910+00
-7.359942-02	1.500616+01	-7.584050-02	1.532712+01
-2.652156-03	3.751637+00	-4.810113-02	1.303733+01
-6.961588.02	1.395664+01	-1.935042-03	2.766611+00
-2.448523-03	3.431595+00	-1.046241+01	1.296920+01
		-2.652452-03	3.756677+00

<u>Gain</u>	<u>Roots at Origin</u>
3.28997959+03	2

The converted transfer function in the W-plane is given below, in the root locus format, for comparison:

<u>Zeros</u>	<u>Poles</u>
<u>Real Roots</u>	<u>Real Roots</u>
-1.01412250+00	-6.53702777-01
9.40818782+00	
1.00000000+00	

<u>Complex Roots</u>		<u>Complex Roots</u>	
-9.597832-01	2.218605-01	-9.673757-01	2.288524-01
-3.859638-03	6.245523-01	-3.727558-03	6.374135-01
-1.044968-04	1.381281-01	-9.978886-05	1.390422-01
-1.144988-03	3.657608-01	-4.535049-03	7.035109-01
-1.051548-04	1.512049-01	-2.559173-03	5.745435-01
-1.550528-04	1.495727+00	-7.835739-05	1.111184-01
-7.666606-05	1.105851-01	-4.991610-01	4.581694-01
-4.303621-03	6.845458-01	-1.085303-04	1.514084-01

<u>Gain</u>	<u>Roots at Origin</u>
4.33835984-05	2

DISCUSSION

The stability analysis results presented in this discussion include both S- and W-plane frequency response data displayed by the graphical gain versus phase method. The W-plane technique is used for the sampled-data TVC DAP and the S-plane is used for the continuous-data SCS autopilot.

As an aide in reading the plots, numbers are used to indicate consecutive points on opposite sides of the page where plotting discontinuities occur due to use of a total phase range of only 360 degrees. The frequency parameter is identified near 0 db coordinates, 180° coordinates, and resonance peaks.

Figure 4 through 19 gives the gain-phase plots in the pitch and yaw control channels of the CSM/LM, in a docked mode, for the following SPS propellant loadings: full load, half-full load, quarter-full load and CSM 104/LM-3 load. These plots are given for the CSM/LM TVC DAP in the W-plane. Each case contained three slosh modes and the first three spacecraft bending modes. The propellant and spacecraft weights used in the CSM-104/LM-3 configuration are approximate weights which are based on the mass properties published in reference 2 for the CSM-103/LM-3 configuration.

A gain-phase plot of the uncompensated spacecraft system precedes each compensated plot for comparison purposes. The stability margins for this set of cases were found to be quite similar. Gain margins varied from 5.8 db for the full case (figure 5) to 5.1 db for the quarter-full cases (figures 13 and 15). The phase margins were also nearly constant varying from a low 41.2 degrees for the half-full cases (figures 9 and 11) to a high of 41.5 degrees for the quarter-full cases. The margins in the pitch and yaw channels were the same to the nearest tenth of a decibel (or degree) except in the full cases, where the yaw channel gain margin was 0.2 db lower than the pitch channel. The quarter-full loadings were the only cases to have resonance peaks above the -7 db coordinates. The first slosh modes on these two plots (figures 13 and 15) are approximately -2 db. Figures 13 and 15 demonstrate that there would have been ample phase margins had these resonant responses crossed the 0 db line. All bending modes for the above cases were attenuated to a minimum of 70 db below the amplitude required for instability. Although the rigid body gain margins are somewhat smaller than expected, they are judged to be adequate due to only minor uncertainty in the math model data that affects these margins.

CSM/IM SCS autopilot gain-phase plots in the S-plane are given in figures 20 through 27. These plots are for the same set of propellant loadings used with the TVC DAP. The SCS analysis was also performed for the spacecraft pitch and yaw control channels. The slosh and bending modes were phase-stabilized for this autopilot; therefore, for some propellant loadings the modes peaked above the 0 db coordinate at or near the resonance frequencies. The rigid body gain margins varied from 13 db for the quarter-full loadings (figures 24 and 25) to 24 db for the CSM-104/IM-3 loads (figures 26 and 27). Rigid body phase margins remained nearly constant varying from 44 degrees to 47 degrees. The first slosh modes peaked above 0 db in all cases except the full load cases (figures 20 and 21) which had resonance peaks to -4 db with ample phase margin if crossover would have occurred. The first and second slosh modes of the quarter-full cases peaked above 0 db in both the pitch and yaw channels. The phase margins for the first slosh modes of these loadings were approximately 10 degrees in both channels. Second mode margins were larger with 33 and 40 degrees of margin in both channels. These first slosh mode phase margins are considered to be lower than desirable, but acceptable due to the extremely slow divergence rates associated with unstable sloshing in the Apollo spacecraft. The first slosh mode phase margins for the half-full cases were 20 degrees (figures 22 and 23). CSM-104/IM-3 first slosh modes were quite large at a 68 degrees. The first bending mode in the pitch channel of the quarter-full case was the only bending mode to peak above 0 db having a phase margin of 120 degrees. The first bending mode in the pitch channel of the other cases peaked to approximately -5, but in each case the phase margin, if it had peaked above 0 db, would have been quite large.

A stability analysis was performed in the pitch and yaw channels of the TVC DAP, and SCS autopilot, for the CSM alone, with propellant loadings of full, half-full, and quarter-full. Figures 28 through 39 give the uncompensated and compensated gain-phase plots for these loadings. The plots are frequency responses in the W-plane. Each case included one slosh mode and three bending modes. The rigid body margins varied from 9 db to 11 db and the phase margins remained nearly constant at 49 degrees. The pole-zero configuration of the slosh mode canceled for the CSM full cases (figures 29 and 31). Slosh mode phase margins for the half-full and quarter-full cases were 45 and 31 degrees respectively (see figures 33, 35, 37, and 39). The first bending modes of the quarter-full cases were attenuated by at least 35 db below the amplitude required for instability. Resonance peaks for modes in other cases were 50 db or more below unity gain.

Gain-phase plots for the CSM alone SCS autopilot are presented in figures 40 through 45. This analysis is performed in the S-plane. The

following SPS propellant loadings were used: full-load, half-full load, and quarter-full load. The slosh mode of the fully loaded CSM in the pitch channel is a pole before zero mode in the airframe transfer function, which is much more difficult to compensate for by use of control filter dynamics. Figure 40 shows that this case has a gain margin of only 7.6 db. The rigid body gain and phase margins for this propellant load are 23 db and 31 degrees. The pole and zero for the slosh mode in the yaw channel of the fully loaded CSM (figure 41) was canceled by the digital program used in the analysis. Rigid body gain and phase margins were 25 db and 28 degrees respectively for this case. CSM half-full rigid body margins in each channel were 23 db and 32 degrees (figures 42 and 43). The slosh mode peaked to -3 db, but there would have been adequate phase margin had it crossed the 0 db line. The CSM quarter load rigid body margins were 20 db and 35 degrees in each channel with a slosh mode phase margin of 36 degrees (figures 44 and 45). All bending modes with this autopilot were attenuated to at least 40 db below unity gain, except for the quarter-full yaw plane case. The gain margins of the first three bending modes for this case were 21 db, 24 db, and 29 db.

A summary of significant stability margins computed in this analysis are presented in Table III.

CONCLUSIONS

Stability data for nominal Apollo spacecraft systems are presented for all cases of SPS powered flight where bending data existed. Nominal bending margins were found to be adequate in all cases. Rigid body gain margin was found to be somewhat lower than expected for the CSM/LM docked configuration under DAP control. The gain at this low frequency would only be affected by very minor uncertainty in the data; therefore, they are judged to be adequate. The sloshing propellant margins were found to be rather low for the CSM/LM with half-full and quarter-full propellant loadings using the SCS autopilot. Due to very small residue in unstable slosh poles for the Apollo control systems these low phase margins are not expected to present any significant stability problem. This position has been substantiated by time domain simulations performed at North American Rockwell Corporation under sponsorship of the Guidance and Control Division.

REFERENCES

1. Internal Letter North American Aviation. "Design Analysis of Block II Backup TVC Autopilot." December 11, 1967.
2. Mass Properties Data Book. NASA SNA-8-D-027, Vol. III, March 1968.
3. CSM/LM Spacecraft Operational Data Book. CSM Data Book, NASA SNA-8-D-027, Vol. I, May 1968.
4. Hutton, R. E.: Mechanical Models for Sloshing in LM Ascent and Descent Tanks, TRW. March 22, 1966.
5. Guidance System Operations Plan for Manned CM Earth Orbital and Lunar Missions Using Program COLOSSUS, Section 3 CSM Digital Autopilots. April 1968.
6. Gardiner, R. A.: CSM TVC DAP filter for S/C 101 and subsequent, MSC memorandum. June 27, 1968.
7. Cox, K. J.: Status of NR redesign of CSM/LM TVC system. July 26, 1968.
8. Michel, W. B.: Description of Digital Programs Available in Systems Analysis Branch, MSC memorandum. January 1966.
9. Bone, E. D.: Program Y001 Control Systems Analysis, NASA MSC. August 1968.
10. Tou, Julius T.: Digital and Sampled Data Control Systems. McGraw-Hill Book Company, 1959.
11. Smith, Emery E., Jr.: Stability Analysis of Apollo Block II CSM/LM Thrust Vector Control Systems, MSC Internal Note No. MSC-EG-69-16.

TABLE I

PARAMETERS USED IN THE ANALYSIS

Actuation System and SCS Electronics

<u>Symbols</u>	<u>Units</u>	<u>Nominal Values</u>	
		<u>Pitch</u>	<u>Yaw</u>
R	ft	0.9875	1.032
K	1/sec	0.09	0.09
τ_1	sec/rad	0.02	0.02
τ_2	sec/rad	0.0333	0.0333
K	rad/rad	1.0	1.0
K_A	lb/ft	3.192×10^6	3.196×10^6
K_L	lb/ft	0.984×10^6	1.302×10^6
K_T	lb/ft	1.86×10^6	1.296×10^6
J_A	ft-lb-sec ²	69.6625	65.4884
B_B	ft-lb-sec	1249.9994	1129.30724
K_S	ma/rad	20,000	20,000
* K_C	ft-lbs/ma	2.9	2.9

CSM/LM half-full and quarter-full $K_C = 2.8$

CSM alone half-full and quarter full $K_C = 2.5$

Table I continued

CSM Alone Pitch Plane

<u>Symbols</u>	<u>Units</u>	<u>Full</u>	<u>$\frac{1}{2}$-Full</u>	<u>$\frac{1}{4}$-Full</u>
M_{J1}	slugs	12	12	12
M_{J2}	"	12	12	12
M_{J3}	"	12	12	12
σ_1	rad/ft	-0.000208	0.0007380	0.0034272
σ_2	"	-0.000603	0.0040224	-0.0117312
σ_3	"	-0.001228	-0.0009096	-0.005094
ϕ_1	ft/ft	0.003960	-0.01351	-0.02588
ϕ_2	"	0.003570	-0.05709	0.06561
ϕ_3	"	0.01628	0.009981	0.02934
ξ_1	N.D.	0.005	0.005	0.005
ξ_2	"	0.005	0.005	0.005
ξ_3	"	0.005	0.005	0.005
ω_1	rad/sec	33.28	36.16	71.53
ω_2	"	37.87	41.45	78.14
ω_3	"	41.43	45.62	80.40
$\sigma_{(IMU)}$	rad/ft	0.000375	0.0002124	0.002502
$\sigma_{(IMU)}$	"	0.000329	0.0014592	-0.0084048
$\sigma_{(IMU)}$	"	0.000132	-0.0002004	-0.0047604

Table I continued

CSM Alone Yaw Plane

<u>Symbols</u>	<u>Units</u>	<u>Full</u>	<u>$\frac{1}{2}$-Full</u>	<u>$\frac{1}{4}$-Full</u>
M_{J1}	slugs	12	12	12
M_{J2}	"	12	12	12
M_{J3}	"	12	12	12
σ_1	rad/ft	-0.000294	0.0018768	0.0081888
σ_2	"	0.000410	0.0007032	0.0074748
σ_3	"	-0.000360	0.0037944	-0.0108624
ϕ_1	ft/ft	0.01451	-0.04017	-0.05328
ϕ_2	"	-0.01163	-0.008830	-0.01395
ϕ_3	"	0.01270	-0.05687	0.01545
ξ_1	N.D.	0.005	0.005	0.005
ξ_2	"	0.005	0.005	0.005
ξ_3	"	0.005	0.005	0.005
ω_1	rad/sec	33.28	36.16	71.53
ω_2	"	37.87	41.45	78.14
ω_3	"	41.43	45.62	80.40
$\sigma_{(IMU)}$	rad/ft	-0.0000917	0.0009240	.0056748
$\sigma_{(IMU)}$	"	-0.0000790	0.0004476	.0026556
$\sigma_{(IMU)}$	"	-0.000206	0.0013908	-.004566

Table I continued

Sloshing Mode DataCSM/LM Pitch Plane

<u>Symbol</u>	<u>Units</u>	<u>Full</u>	<u>$\frac{1}{2}$-Full</u>	<u>$\frac{1}{4}$-Full</u>	<u>CSM-104/LM-3</u>
M_1	slugs	40.56	53.28	49.285	39.82
M_2	"	48.62	48.62	48.62	49.03
M_3	"	17.22	17.22	17.22	14.77
l_1	ft	8.834	12.042	17.966	10.624
l_2	"	-18.654	-16.355	-14.300	-18.54
l_3	"	-13.462	-11.163	-9.093	-13.322
ξ_1	N.D.	0.0007	0.0007	0.0007	0.0007
ξ_2	N.D.	0.0007	0.0007	0.0007	0.0007
ξ_3	N.D.	0.0007	0.0007	0.0007	0.0007
ω_1	rad/sec	2.745	2.9	2.909	2.634
ω_2	"	3.367	3.367	3.367	3.381
ω_3	"	3.723	3.723	3.723	3.738

CSM/LM Yaw Plane

M_1	slugs	40.56	53.28	49.285	39.82
M_2	"	48.62	48.62	48.62	49.03
M_3	"	17.22	17.22	17.22	14.77
l_1	ft	8.834	12.042	17.966	10.624
l_2	"	-18.654	-16.355	-14.300	-18.54
l_3	"	-13.462	-11.163	-9.093	-13.322
ξ_1	N.D.	0.0007	0.0007	0.0007	0.0007
ξ_2	N.D.	0.0007	0.0007	0.0007	0.0007
ξ_3	N.D.	0.0007	0.0007	0.0007	0.0007
ω_1	rad/sec	2.745	2.9	2.909	2.634
ω_2	"	3.367	3.367	3.367	3.381
ω_3	"	3.723	3.723	3.723	3.738

Table I continued

<u>CSM/LM Yaw Plane</u>					
<u>Symbols</u>	<u>Units</u>	<u>Full</u>	<u>$\frac{1}{2}$-Full</u>	<u>$\frac{1}{4}$-Full</u>	<u>CSM-104/LM-3</u>
M_{J1}	slugs	12	12	12	12
M_{J2}	"	12	12	12	12
M_{J3}	"	12	12	12	12
σ_1	rad/ft	-0.0048	0.0060	-0.0048	-0.0048
σ_2	"	-0.0072	-0.0072	-0.0084	-0.0072
σ_3	"	-0.0036	-0.0024	-0.00084	-0.0036
ϕ_1	ft/ft	0.0329	-0.0521	0.0440	0.0329
ϕ_2	"	0.0518	0.0549	0.0763	0.0518
ϕ_3	"	0.0292	0.0272	0.0144	0.0292
ξ_1	N.D.	0.005	0.005	0.005	0.005
ξ_2	"	0.005	0.005	0.005	0.005
ξ_3	"	0.005	0.005	0.005	0.005
ω_1	rad/sec	13.06901	13.82301	14.0744	13.06901
ω_2	"	14.19999	14.57699	14.9540	14.19999
ω_3	"	15.33096	15.51947	18.6611	15.33096
$\sigma_{(IMU)}$	rad/ft	-0.0036	0.0048	-0.0048	-0.0036
$\sigma_{(IMJ)}$	"	-0.0060	-0.0048	-0.0072	-0.0060
$\sigma_{(IMU)}$	"	-0.0024	-0.0024	-0.0012	-0.0024

Table I continued

Rigid BodyCSM/LM Pitch Plane

<u>Symbols</u>	<u>Units</u>	<u>Full</u>	<u>$\frac{1}{2}$-Full</u>	<u>$\frac{1}{4}$-Full</u>	<u>CSM-104/LM-3</u>
M	slugs	2665.1	2214.31	1906.8	2644.1
M _e	slugs	27.795	27.795	27.795	27.795
l _e	ft	0.342	0.342	0.342	0.342
l _x	ft	17.179	19.479	21.533	17.047
I _A	slug-ft ²	493507	386747	333107	484771
I _e	slug-ft ²	236.0	236.0	236.0	236.0
F	lbs	20,000	20,000	20,000	20,000

CSM/LM Yaw Plane

M	slugs	2665.1	2214.3	1906.8	2644.1
M _e	slugs	27.795	27.795	27.795	27.795
l _e	ft	0.200	0.200	0.200	0.200
l _x	ft	17.179	19.479	21.533	17.047
I _A	slug-ft ²	493499	396747	338966	489609
I _e	slug-ft ²	245.9	245.9	245.9	245.9
F	lbs	20,000	20,000	20,000	20,000

Table I continued.

Bending ParametersCSM/LM Pitch Plane

<u>Symbols</u>	<u>Units</u>	<u>Full</u>	<u>$\frac{1}{2}$-Full</u>	<u>$\frac{1}{4}$-Full</u>	<u>CSM-104/LM-3</u>
M _{J1}	slugs	12	12	12	12
M _{J2}	"	12	12	12	12
M _{J3}	"	12	12	12	12
σ_1	rad/ft	0.0084	-0.0034	0.0096	0.0034
σ_2	"	-0.0048	-0.0060	-0.0048	-0.0048
σ_3	"	-0.0012	-0.0024	-0.00036	-0.0012
ϕ_1	ft/ft	-0.0602	0.0676	-0.0819	-0.0602
ϕ_2	"	0.0337	0.0474	0.0451	0.0337
ϕ_3	"	0.0159	0.0309	-0.0110	0.0159
ξ_1	N.D.	0.005	0.005	0.005	0.005
ξ_2	"	0.005	0.005	0.005	0.005
ξ_3	"	0.005	0.005	0.005	0.005
ω_1	rad/sec	13.06901	13.82301	14.0744	13.06901
ω_2	"	14.19999	14.57699	14.9540	14.19999
ω_3	"	15.33096	15.51947	18.6611	15.33096
σ (IMU)	rad/ft	0.0072	-0.0072	0.0084	0.0072
σ (IMU)	"	-0.0036	-0.0048	-0.0048	-0.0036
σ (IMU)	"	-0.0072	-0.0012	-0.00024	-0.0072

Table I continued

<u>C/S/M Alone Pitch Plane</u>				
<u>Symbols</u>	<u>Units</u>	<u>Full</u>	<u>$\frac{1}{2}$-Full</u>	<u>$\frac{1}{4}$-Full</u>
M	slugs	1882.1	1263.8	978.6
M_e	slugs	27.795	27.795	27.795
l_e	ft	0.342	0.342	0.342
l_x	ft	8.634	9.394	10.406
I_A	slug-ft ²	80732	63948	60623
I_e	slug-ft ²	236.0	236.0	236.0
F	lbs	20,000	20,000	20,000

<u>C/S/M Alone Yaw Plane</u>				
M	slugs	1882.1	1263.8	978.6
M_e	slugs	27.795	27.795	27.795
l_e	ft	0.200	0.200	0.200
l_x	ft	8.634	9.394	10.406
I_A	slug-ft ²	80741	69014	60698
I_e	slug-ft ²	245.9	245.9	245.9
F	lbs	20,000	20,000	20,000

Table I continued

GSM Alone Pitch Plane

<u>Symbol</u>	<u>Units</u>	<u>Full</u>	<u>$\frac{1}{2}$-Full</u>	<u>$\frac{1}{4}$-Full</u>
M	slugs	40.56	53.28	55.24
l	ft	0.287	1.963	7.418
ξ	N.D.	0.0007	0.0007	0.0007
ω	rad/sec	3.40	3.88	4.42

GSM Alone Yaw Plane

M	slugs	40.56	58.28	55.24
l	ft	0.287	1.963	7.418
ξ	N.D.	0.0007	0.0007	0.0007
ω	rad/sec	3.40	3.88	4.42

Gain Factor of TVC DAP for GSM/LM Pitch Plane

<u>Symbol</u>	<u>Units</u>	<u>Full</u>	<u>$\frac{1}{2}$-Full</u>	<u>$\frac{1}{4}$-Full</u>	<u>GSM-104/LM-3</u>
K_z	1/sec ²	0.00284	0.00199	0.00167	0.00279

Gain Factor of TVC DAP for GSM/LM Yaw Plane

K_z	1/sec ²	0.00284	0.00204	0.00169	0.00281
-------	--------------------	---------	---------	---------	---------

Gain Factor of TVC DAP for GSM Alone Pitch Plane

K_z	1/sec ²	4.10982	3.30924	2.87380
-------	--------------------	---------	---------	---------

Gain Factor of TVC DAP for GSM Alone Yaw Plane

K_z	1/sec ²	4.10982	3.30924	2.87380
-------	--------------------	---------	---------	---------

TABLE II

LIST OF SYMBOLS

Actuation System and SCS Electronics

B_{θ}^{\prime}	Actuator damping factor, ft-lb-sec
J_A^{\prime}	Rotary inertia of actuator clutch-bull gear assembly, ft-lb-sec ²
K_A	Actuator arm stiffness, lb/ft
K_C	Actuator clutch gain, ft-lb/ampere
K_L	Thrust strut plus gimbal ring stiffness, lb/ft
K_S	Servo amplifier gain, amp/rad
K_T	Actuator mount stiffness, lb/ft
K	Actuator position feedback gain, rad/rad
K	Actuator rate feedback gain, rad/rad/sec
τ_1	Clutch lead time constant, sec
τ_2	Clutch lag time constant, sec

Rigid Body

M	Mass of vehicle without engine and slosh masses, slugs
M_e	Mass of engine, slugs
l_e	Distance from engine hinge point to engine center of mass, ft
l_x	Distance from engine hinge point to vehicle center of mass, ft
I_A	Moment of inertia about vehicle center of mass without engine inertia, ft-lb-sec ²
I_E	Moment of inertia about engine center of mass, ft-lb-sec ²
F	Thrust of engine, lb

Table II continued

Bending Parameters

M_j	Generalized mass of the j^{th} bending mode, slugs
$\sigma_i(x)$	Normalized slope of the i^{th} bending mode
$\phi_i(x)$	Normalized displacement of the i^{th} bending mode at location x , ft/ft
ξ_i	Damping ratio the i^{th} bending mode, n.d.
ω_i	Natural frequency of the i^{th} bending mode, rad/sec

Slosh Parameters

M_j	Mass of the j^{th} slosh mode, slugs
l_i	Distance between vehicle center of mass and attach point of the i^{th} slosh mass, positive when slosh mass attach point is aft of vehicle center of mass, ft
ξ_i	Damping ratio of i^{th} slosh mode, n.d.
ω_i	Natural frequency of the i^{th} slosh mode, n.d.

TABLE III

SUMMARY OF SIGNIFICANT STABILITY MARGINSThrust Vector Control Digital AutopilotRigid Body

	Full		$\frac{1}{2}$ -Full		$\frac{1}{4}$ -Full		CSM-104/LM-3	
	Gain	Phase	Gain	Phase	Gain	Phase	Gain	Phase
CSM/LM Pitch Channel	5.8	41.3	5.6	41.2	5.1	39.6	5.7	41.5
CSM/LM Yaw Channel	5.6	41.3	5.6	41.2	5.1	39.7	5.7	41.5
CSM Pitch Channel	9.4	48.2	11.1	49	9.4	48.7		
CSM Yaw Channel	11.2	49.2	10.5	49	9.4	48.7		
	<u>Slosh</u>							
CSM Pitch Channel	--	--	--	45	--	31.3	--	--
CSM Yaw Channel	--	--	--	45	--	30.2	--	--

Table III continued

Stabilization Control System

Rigid Body

	<u>Full</u>		$\frac{1}{2}$ -Full		$\frac{1}{4}$ -Full		<u>CSM-104/LM-3</u>	
	Gain	Phase	Gain	Phase	Gain	Phase	Gain	Phase
CSM/LM Pitch Channel	22	47.3	20	46.5	13	43.5	24	47.7
CSM/LM Yaw Channel	22	47.3	20	46.5	14	44	24	47.7
CSM Pitch Channel	23	31	23	31	20	35	--	--
CSM Yaw Channel	25	28	23	33	20	35	--	--

Slosh

CSM/LM Pitch Channel	1)	--	--	--	20	15	--	--	69
	2)	--	--	--	--	33	--	--	--
CSM/LM Yaw Channel	1)	--	--	--	22	15	--	--	69
	2)	--	--	--	--	40	--	--	--
CSM Pitch Channel		--	--	--	--	--	36	--	--
CSM Yaw Channel		--	--	--	--	--	36	--	--

Bending

CSM Yaw Channel	1)	--	--	--	--	21	--	--	--
	2)	--	--	--	--	29	--	--	--
	3)	--	--	--	--	24	--	--	--

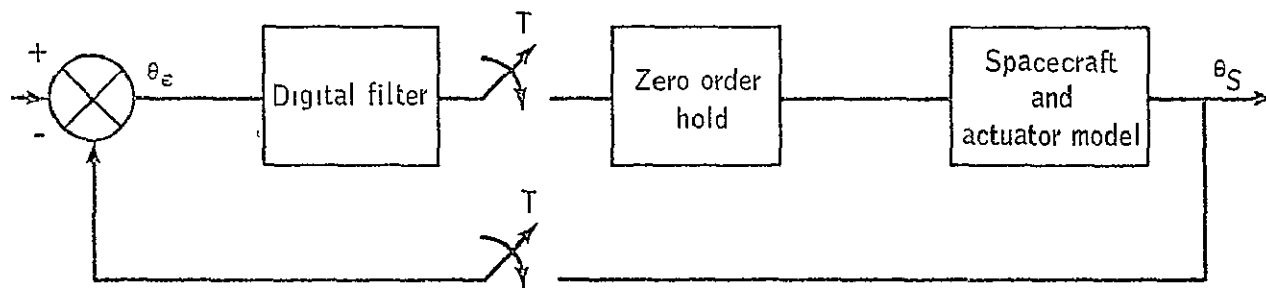
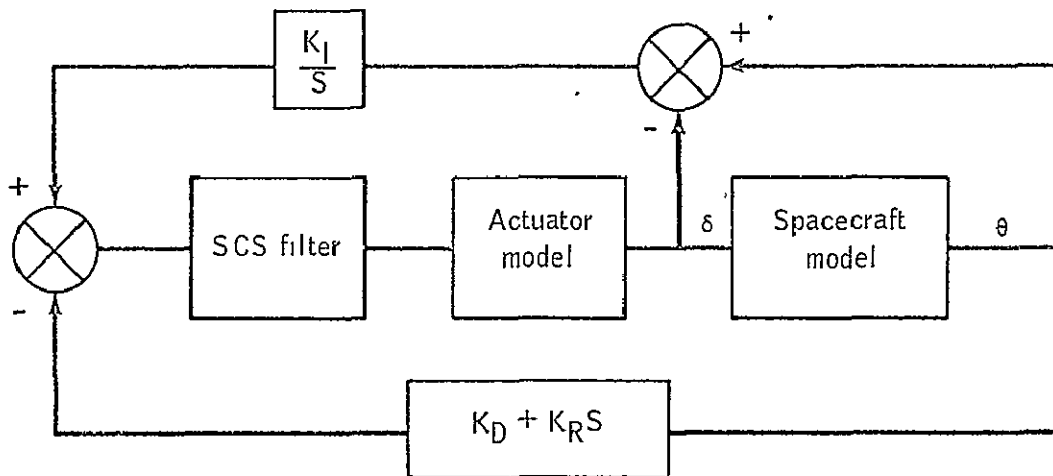


Figure 1. - TVC DAP attitude control system.



	CSM	CSM/LM
$K_D =$	0.4	0.166
$K_R =$	0.3	0.895
$K_I =$	0.03	0.021

Figure 2. - Stabilization control system autopilot.

CSM/LN FULL PITCH PLANE

GAIN - PHASE PLOT

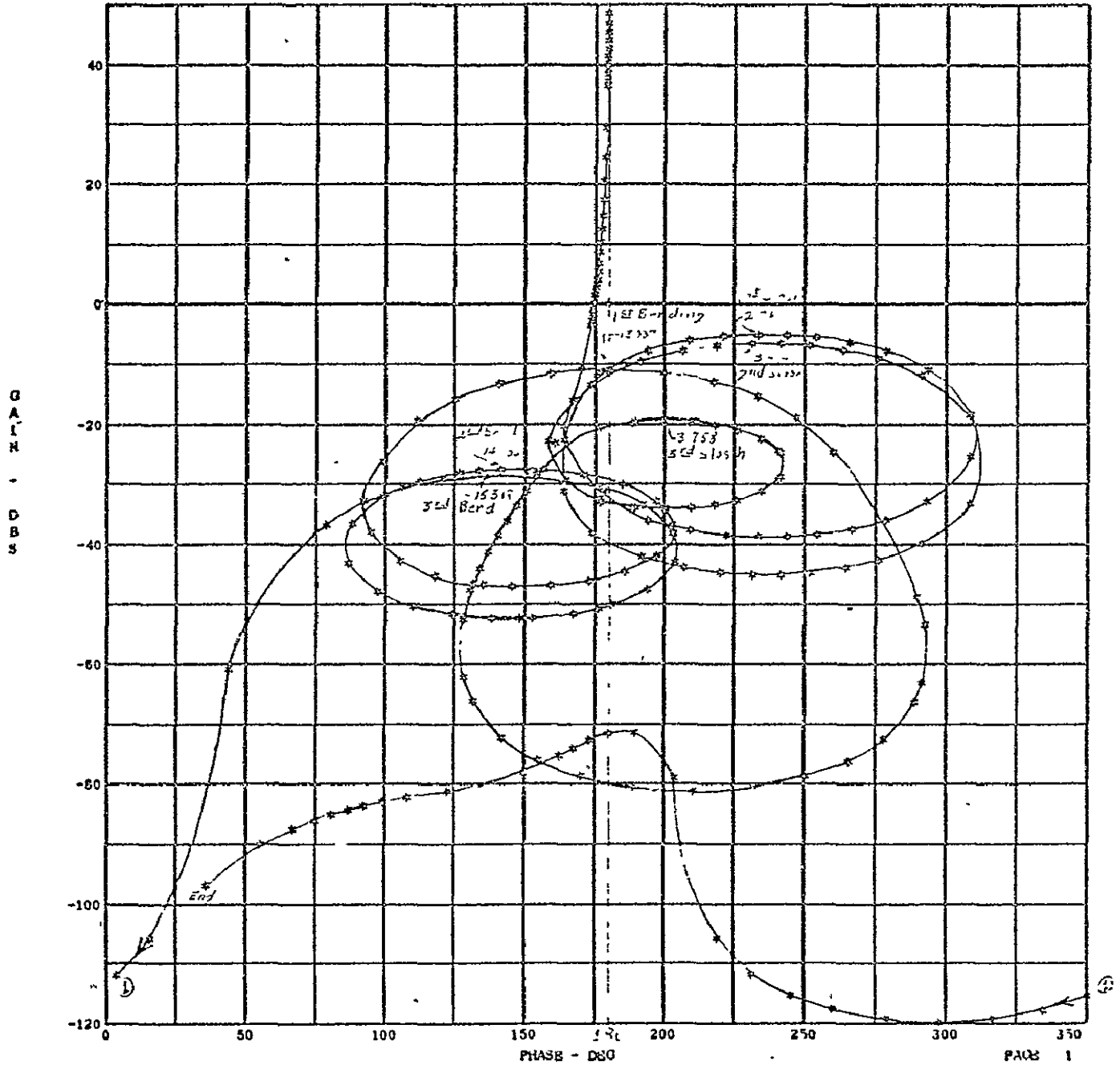


Figure 3
S-PLANE FREQUENCY RESPONSE OF THE
UNCOMPENSATED SYSTEM

CSM/LM FULL PITCH PLANE

GAIN - PHASE PLOT

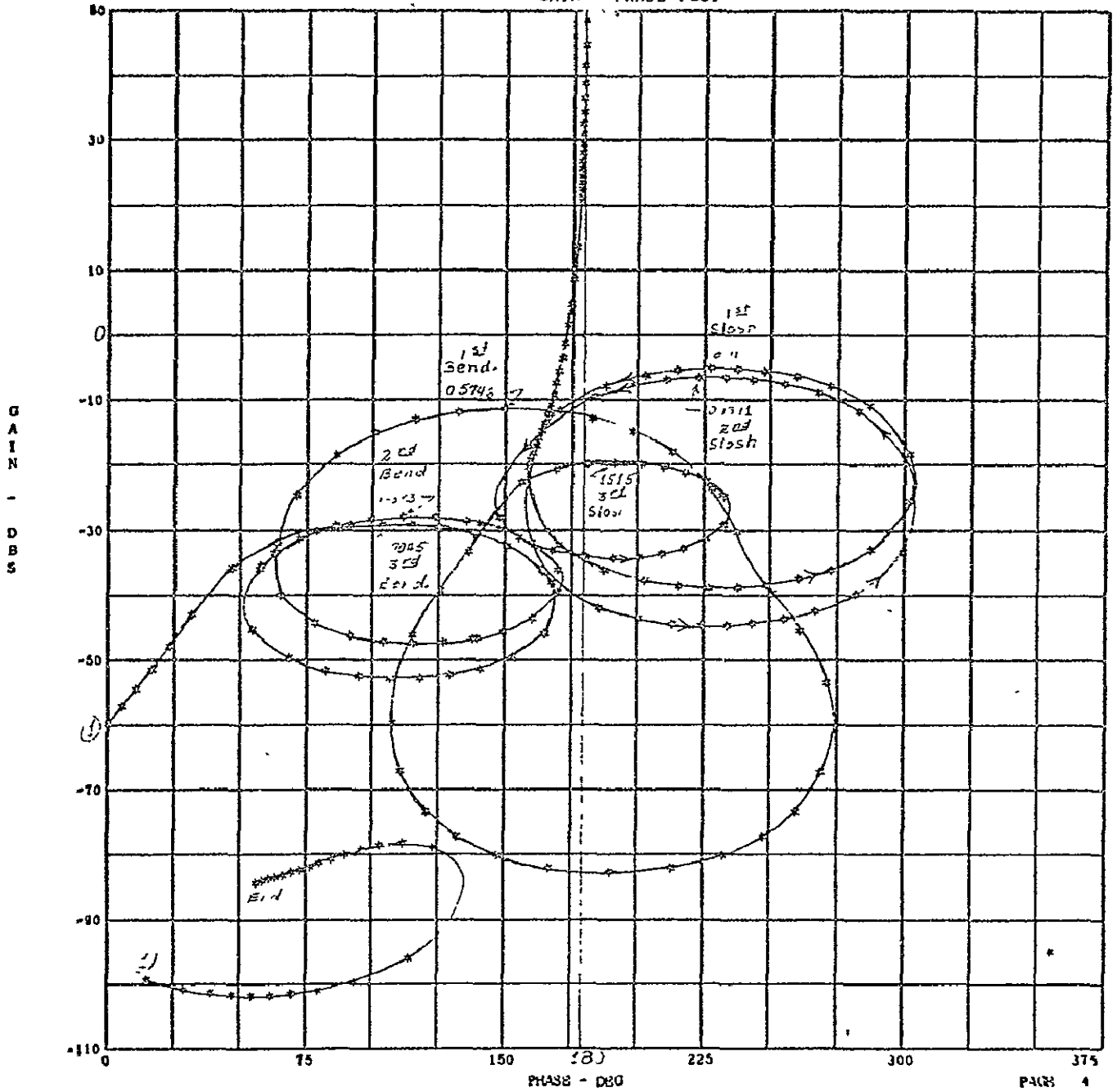


Figure 4

W-PLANE FREQUENCY RESPONSE OF THE UNCOMPENSATED SYSTEM

CSM/L4 FULL PITCH PLANE

GAIN - PHASE PLOT

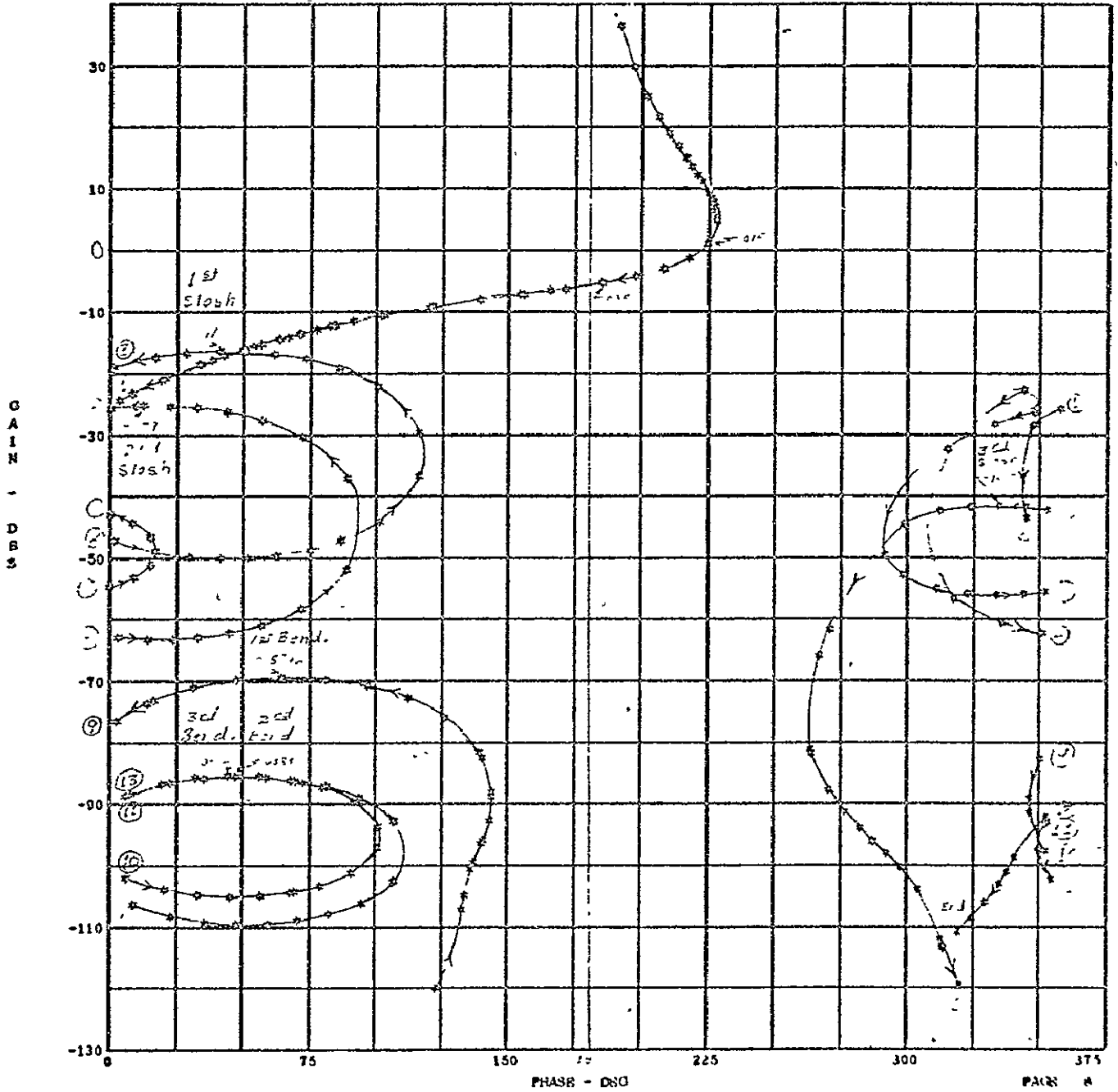


Figure 5

W-PLANE FREQUENCY RESPONSE OF THE COMPENSATED SYSTEM USING THE DAP

CSM/LM PULL, YAW PLANE

GAIN - PHASE PLOT

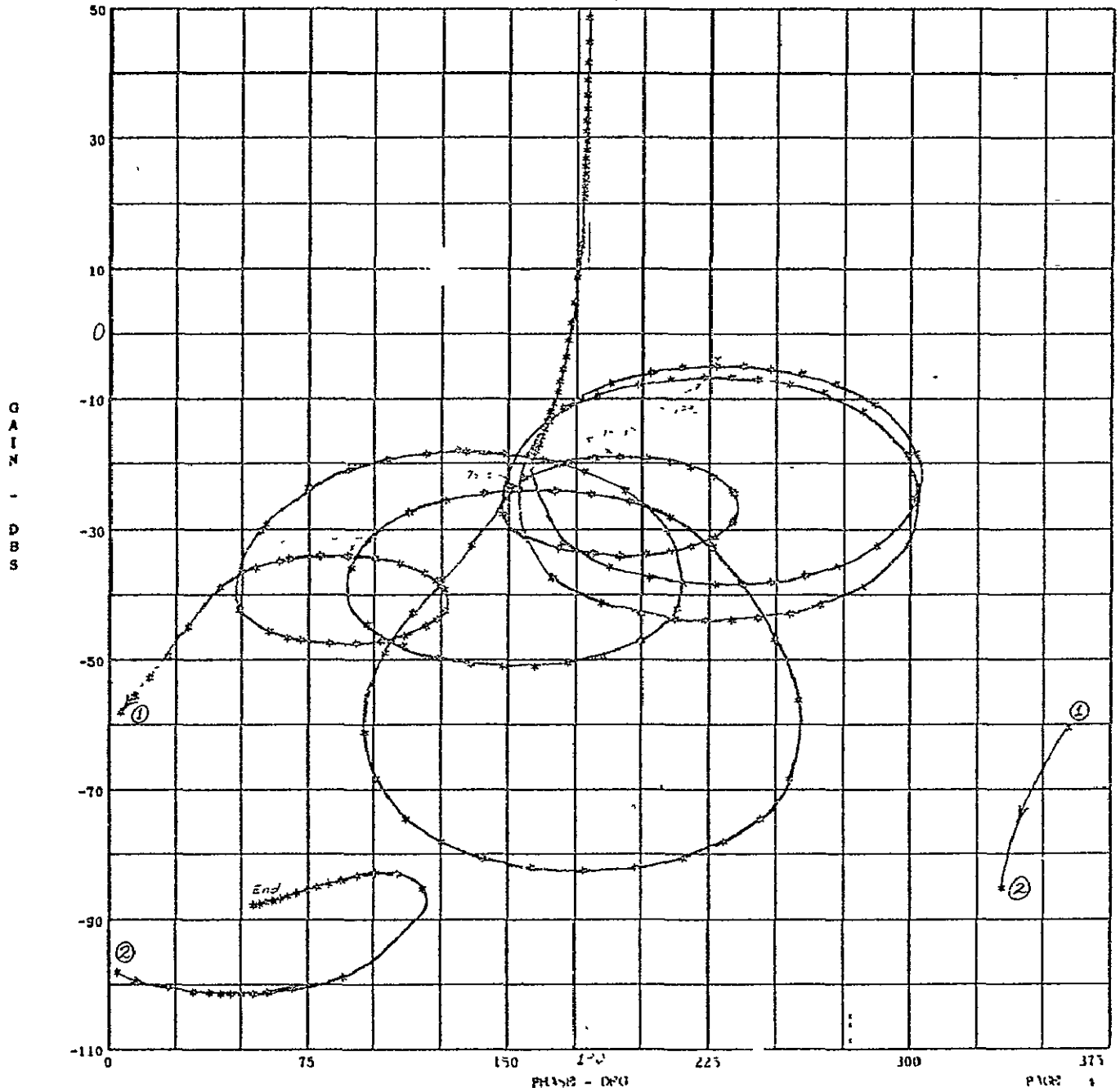


Figure 6
W-PLANE FREQUENCY RESPONSE OF THE
UNCOMPENSATED SYSTEM

Cs4/L4 PJLL, YAW PLANE

GAIN - PHASE PLOT

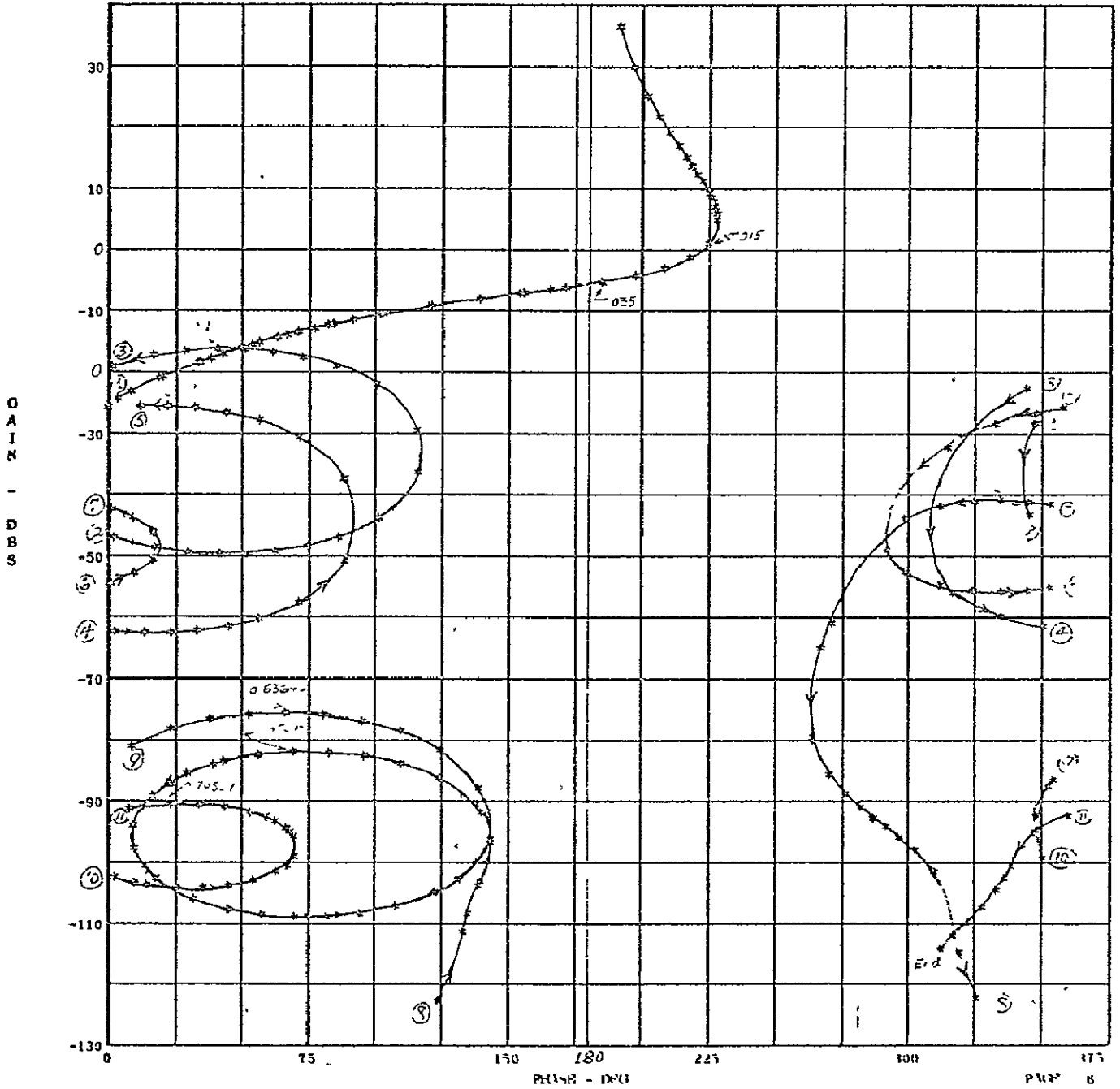


Figure 7

W-PLANE FREQUENCY RESPONSE OF THE COMPENSATED SYSTEM USING THE DAP

CS4/L4 HALP PULL PITCH PLANE

GAIN - PHASE PLOT

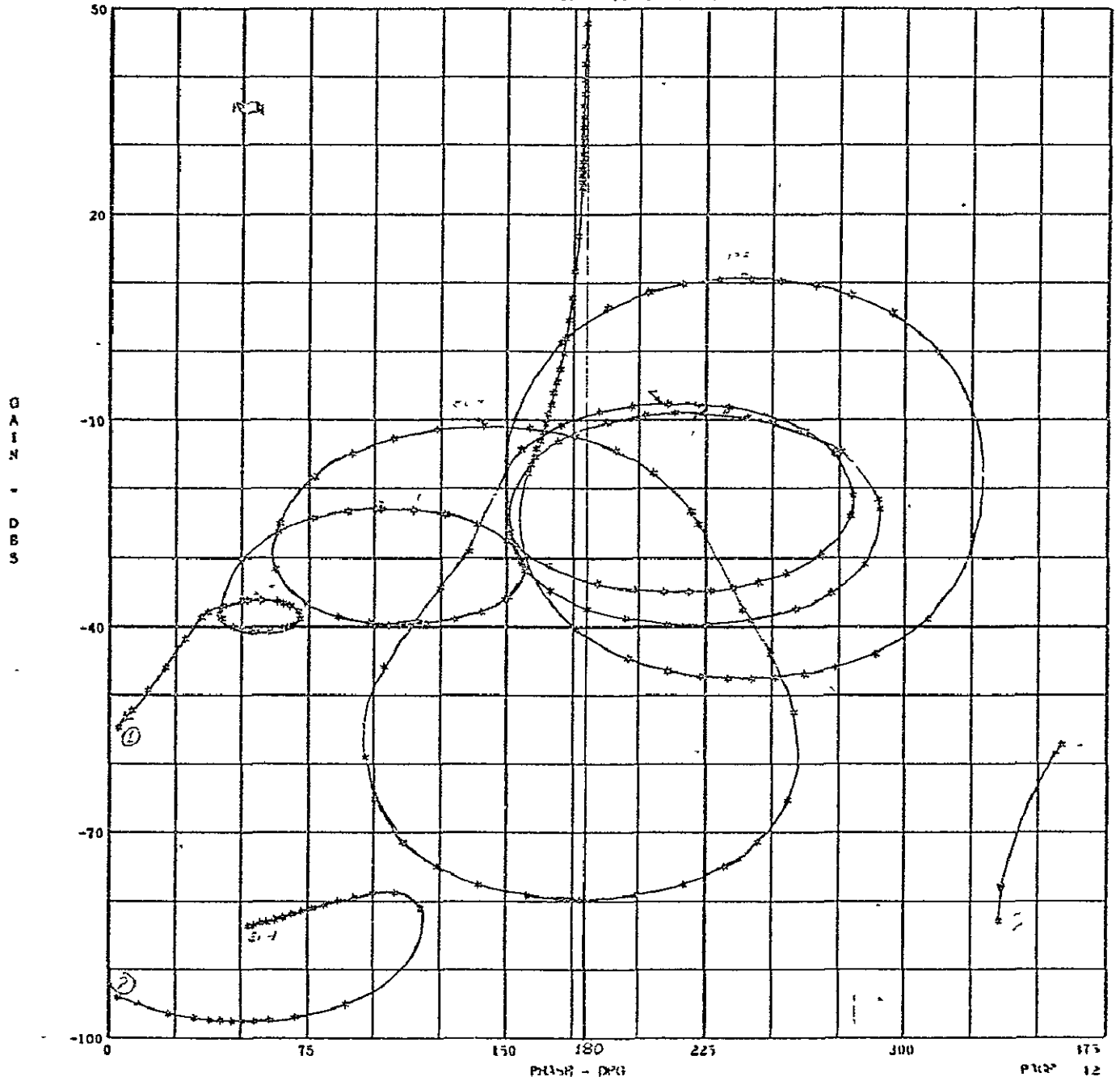


Figure 8
W-PLANE FREQUENCY RESPONSE OF THE
UNCOMPENSATED SYSTEM

CS4/L4 HALF PULL PITCH PLANE
GAIN - PHASE PLOT

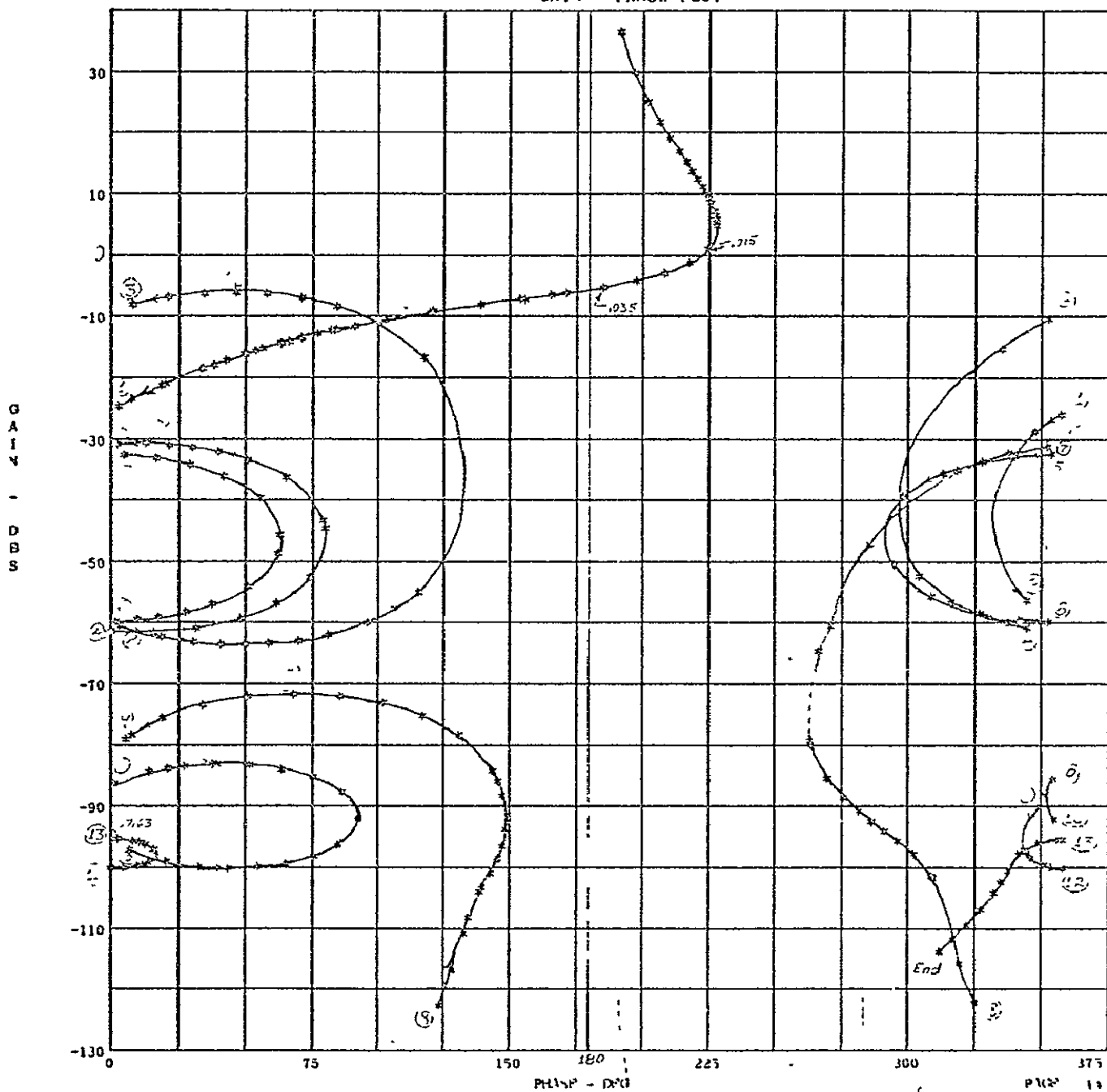


Figure 9
W-PLANE FREQUENCY RESPONSE OF THE
COMPENSATED SYSTEM USING THE DAP

CSM/LM HALF PULL, YAW PLANE

GAIN - PHASE PLOT

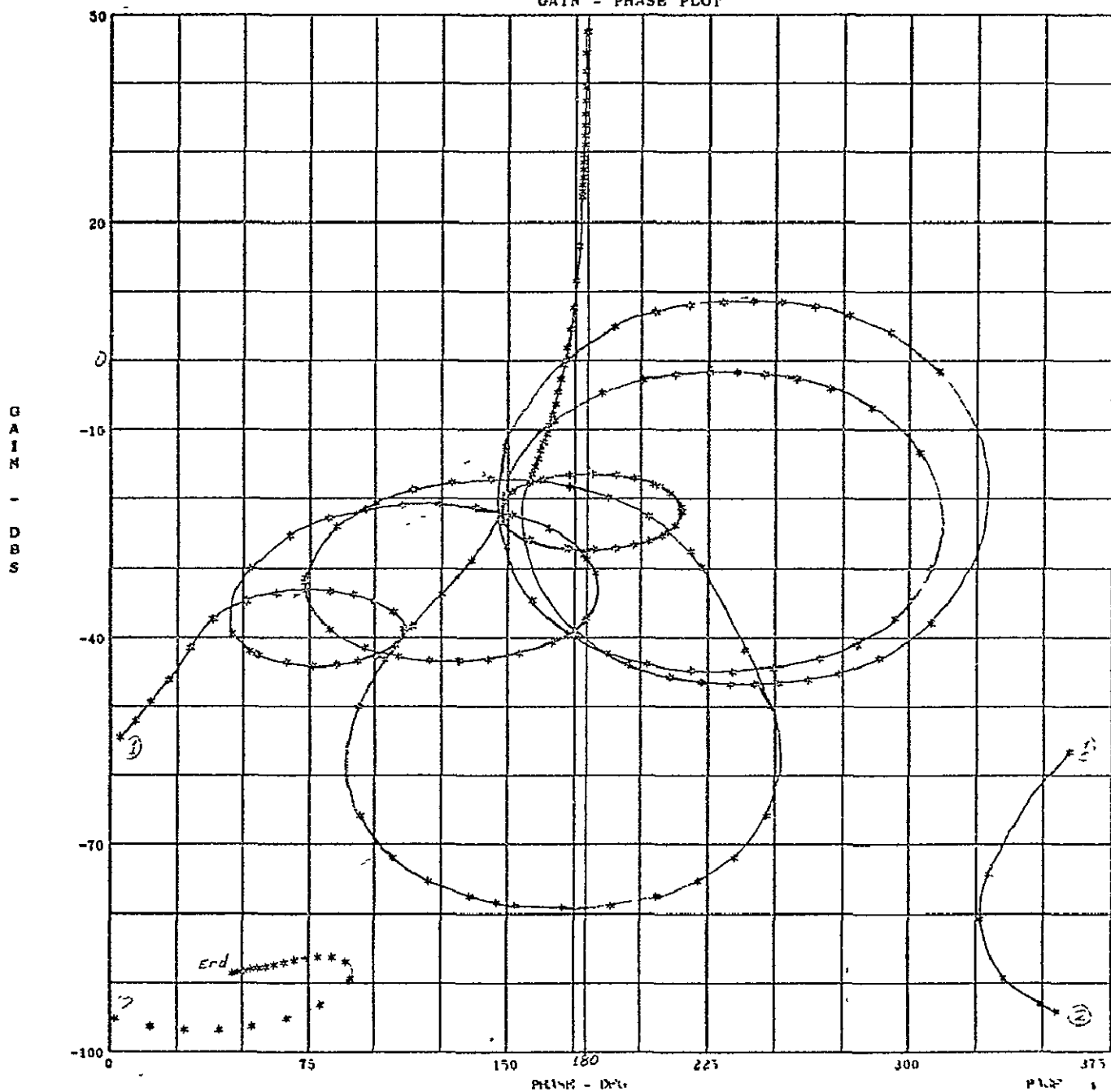


Figure 10
W-PLANE FREQUENCY RESPONSE OF THE
UNCOMPENSATED SYSTEM

CS4/LM HALP PULL, YAW PLANE

GAIN - PHASE PLOT

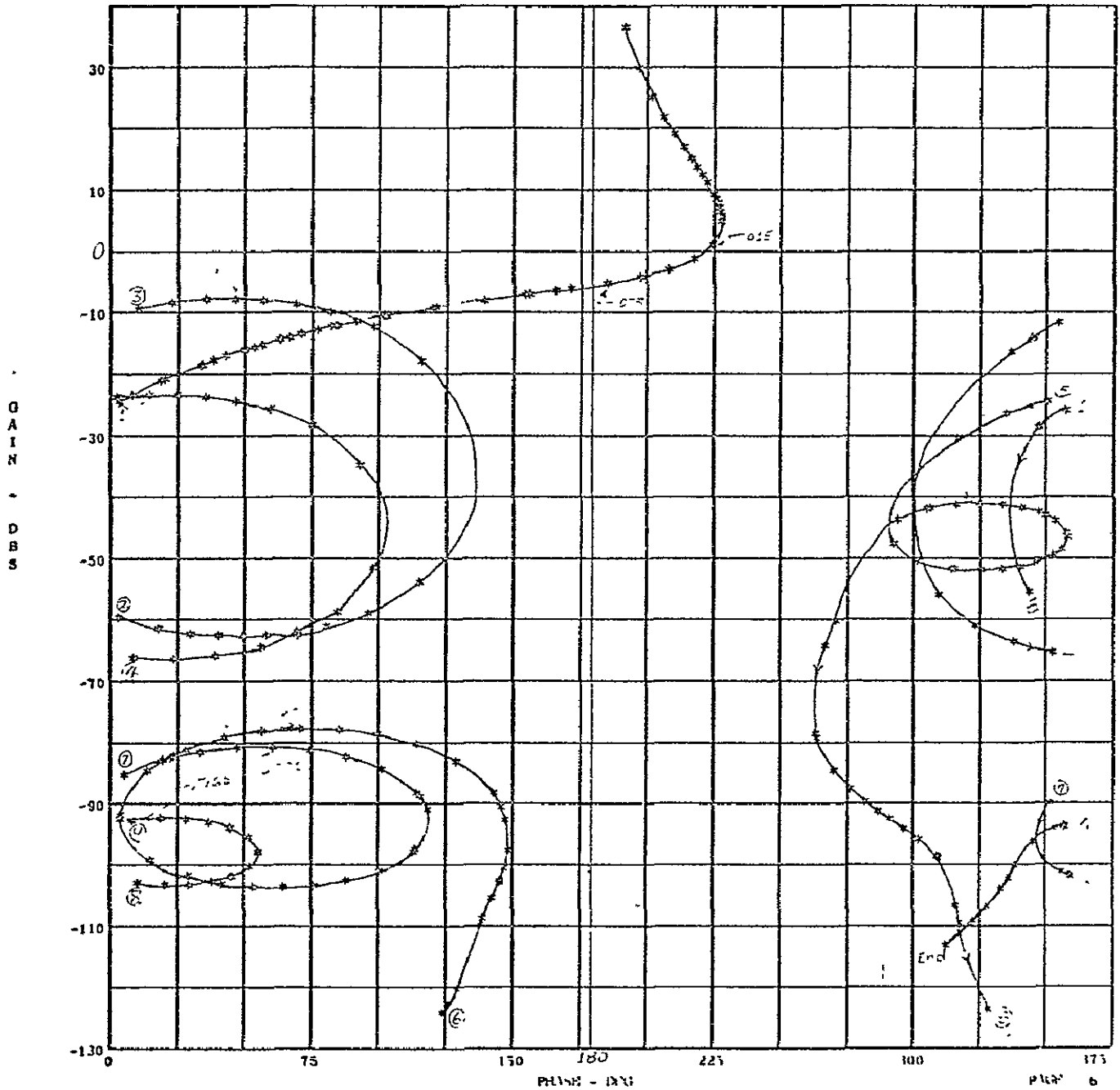


Figure 11

W-PLANE FREQUENCY RESPONSE OF THE COMPENSATED SYSTEM USING THE DAP

CS4/L4 QUARTER LOAD, PITCH PLANE
GAIN - PHASE PLOT

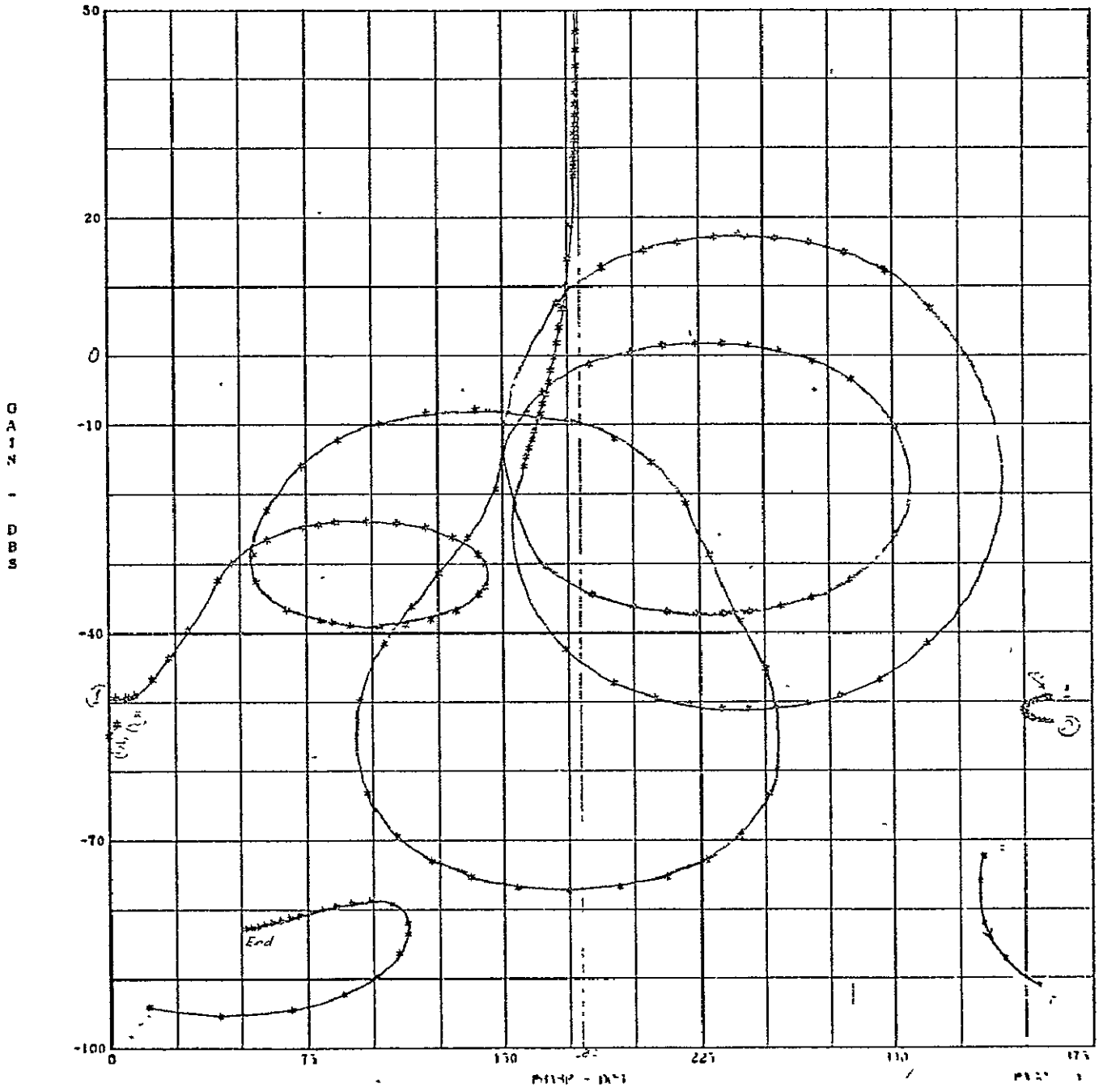


Figure 12
W-PLANE FREQUENCY RESPONSE OF THE UNCOMPENSATED SYSTEM

CS4/L4 QUARTER LOAD, PITCH PLANE
GAIN - PHASE PLOT

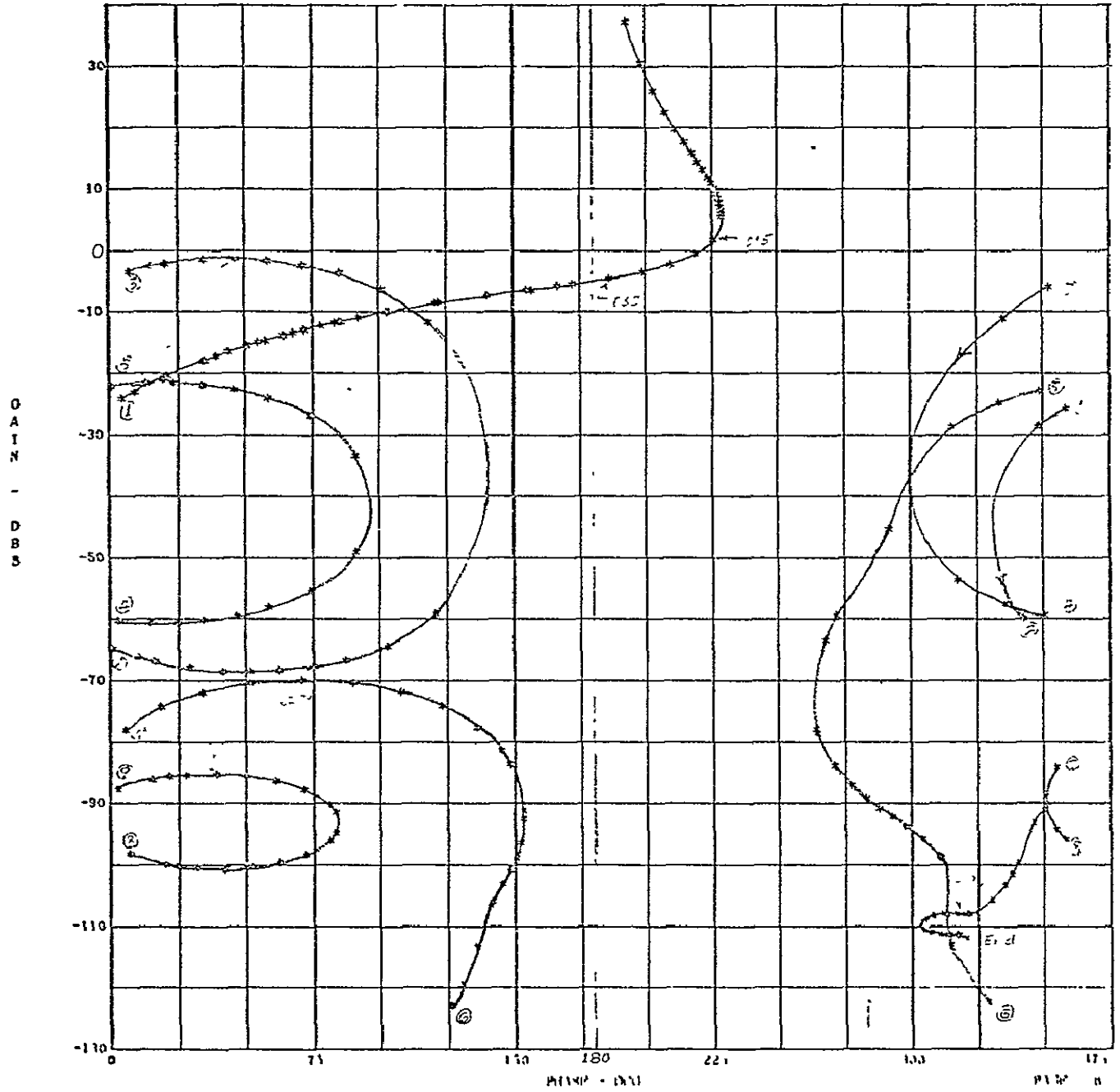


Figure 13
W-PLANE FREQUENCY RESPONSE OF THE COMPENSATED SYSTEM USING THE DAP

CS4/LM 1/4 PULL, YAW PLANE

GAIN - PHASE PLOT

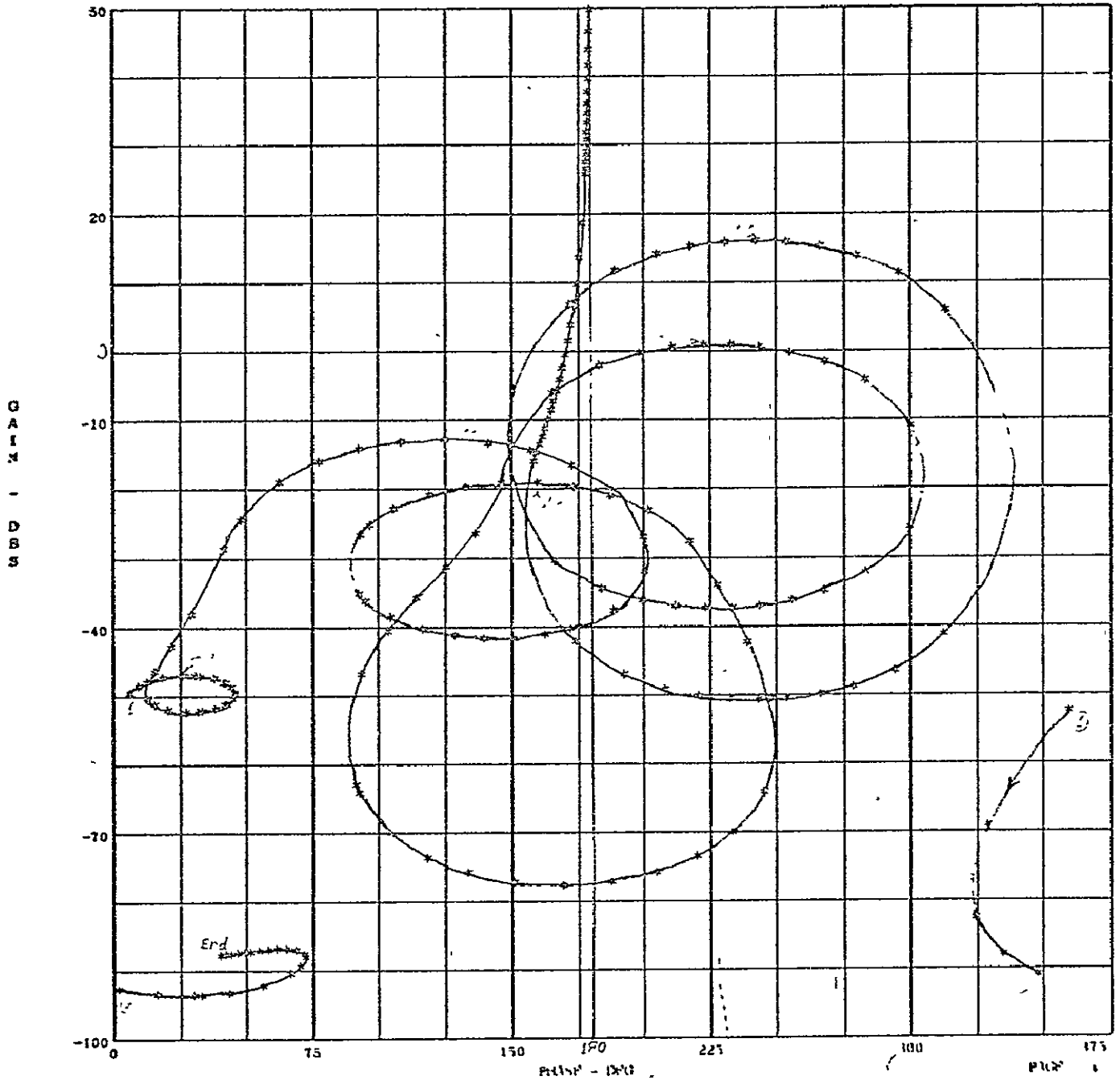


Figure 14
W-PLANE FREQUENCY RESPONSE OF THE
UNCOMPENSATED SYSTEM

CS4/L4 1/4 FULL, YAW PLANE

GAIN - PHASE PLOT

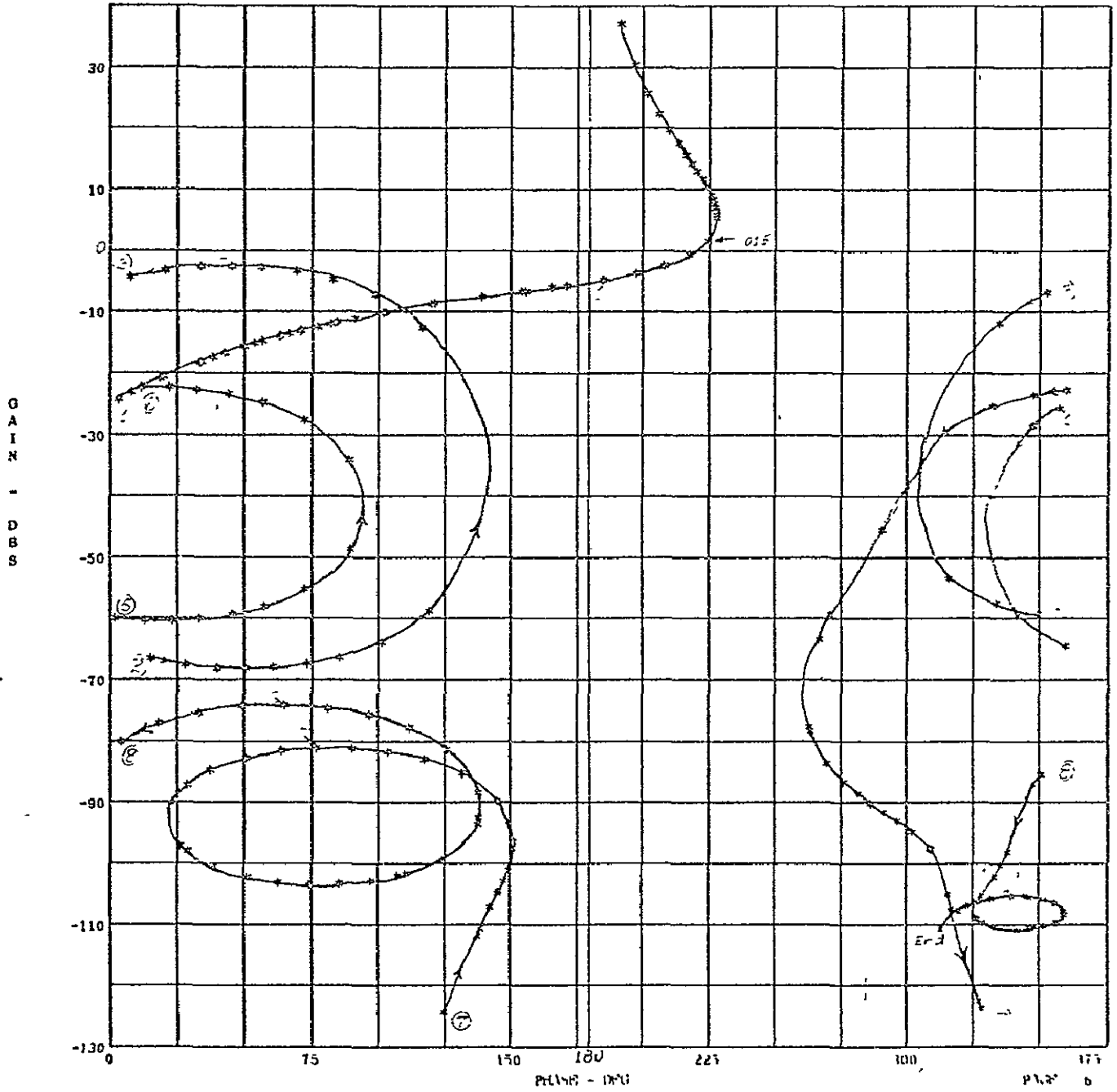


Figure 15
W-PLANE FREQUENCY RESPONSE OF THE COMPENSATED
SYSTEM USING THE DAP

CSM-104/IN-3

LOAD, PITCH PLANE

GAIN - PHASE PLOT

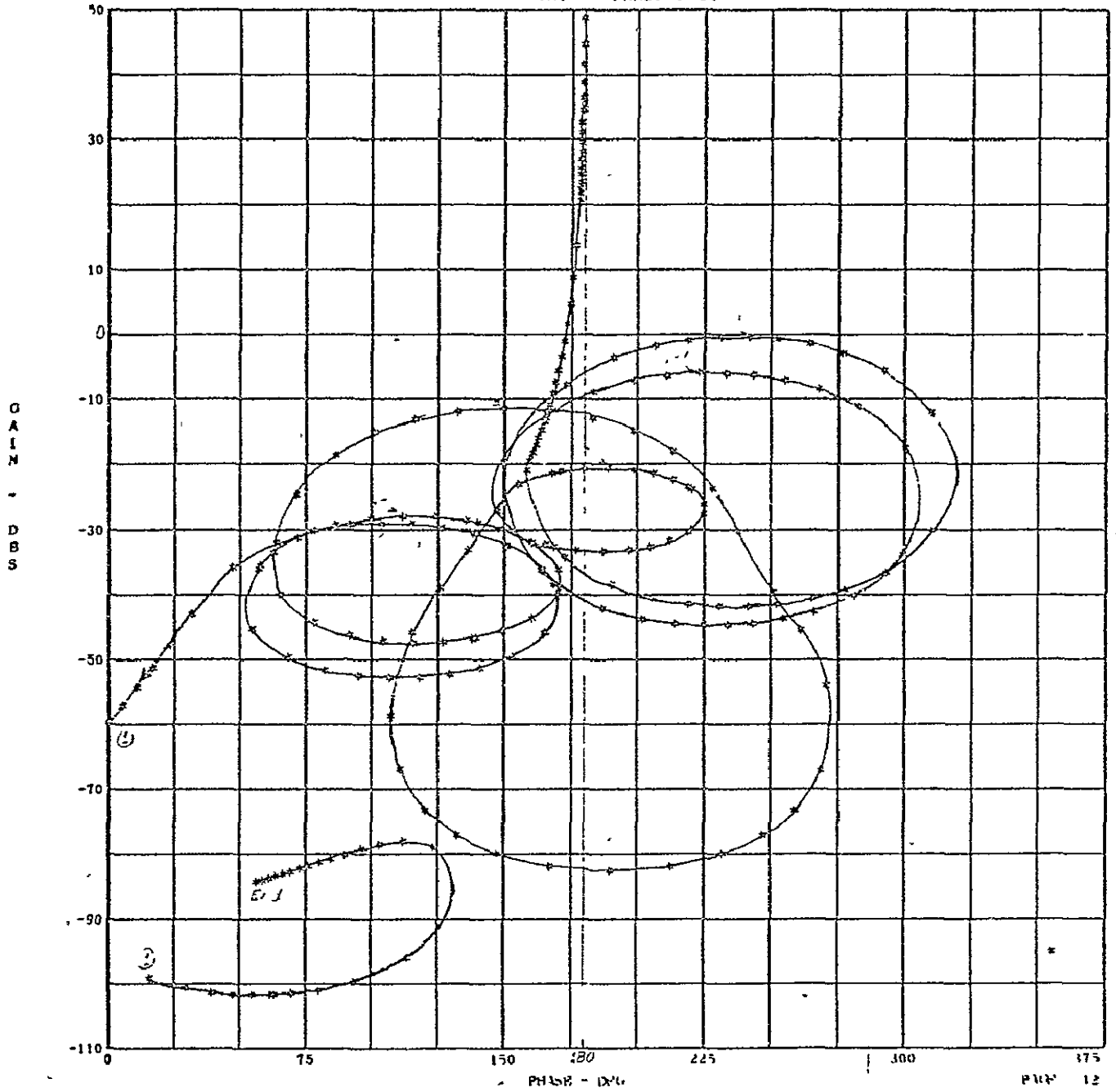


Figure 16
W-PLANE FREQUENCY RESPONSE OF THE
UNCOMPENSATED SYSTEM

CSM-10⁴/LM-3

LOAD, PITCH PLANE

GAIN - PHASE PLOT

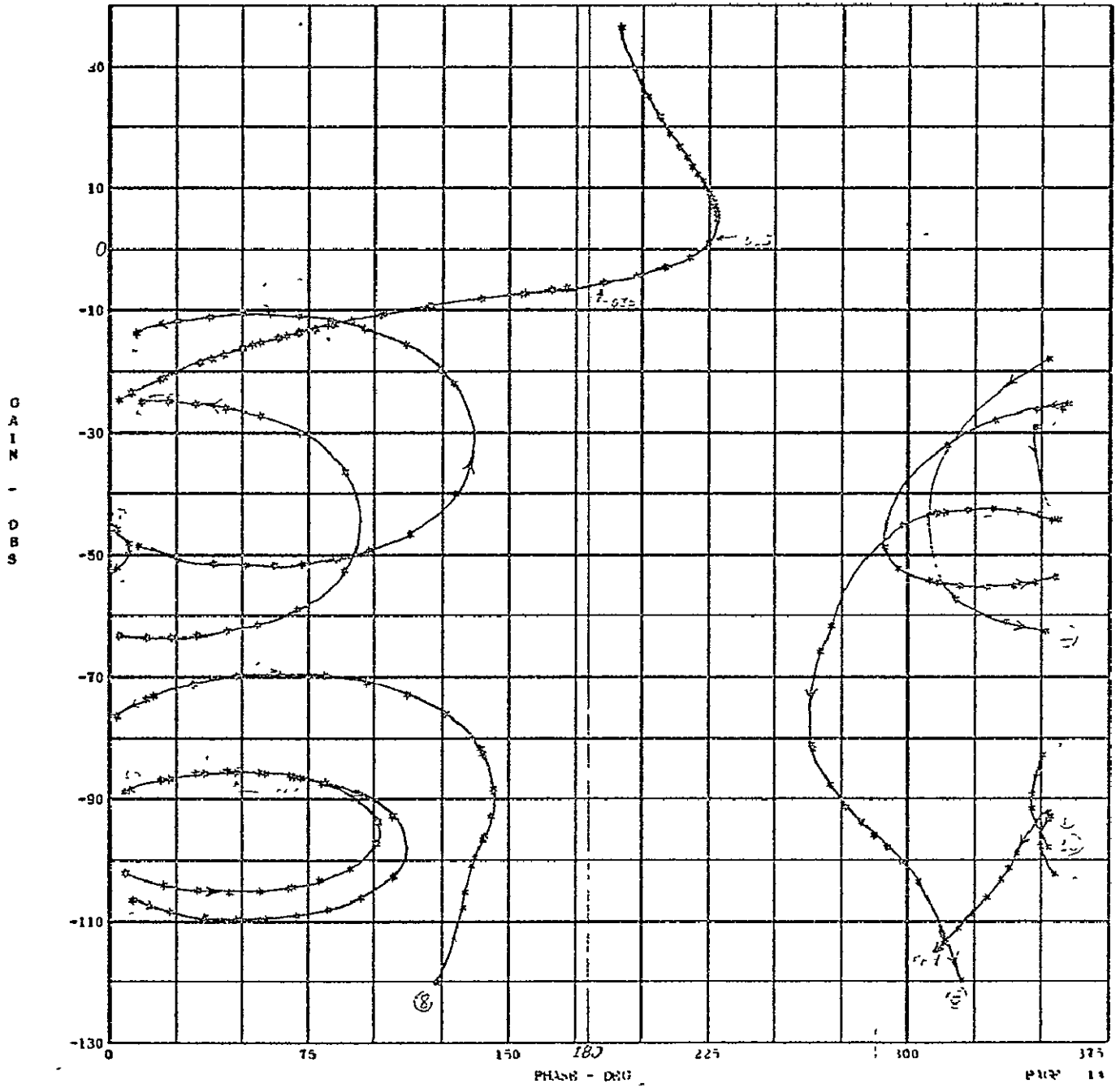


Figure 17
W-PLANE FREQUENCY RESPONSE OF THE COMPENSATED
SYSTEM USING THE DAP

CSM-1-4/IM-3 LOAD, YAW PLANE

GAIN - PHASE PLOT

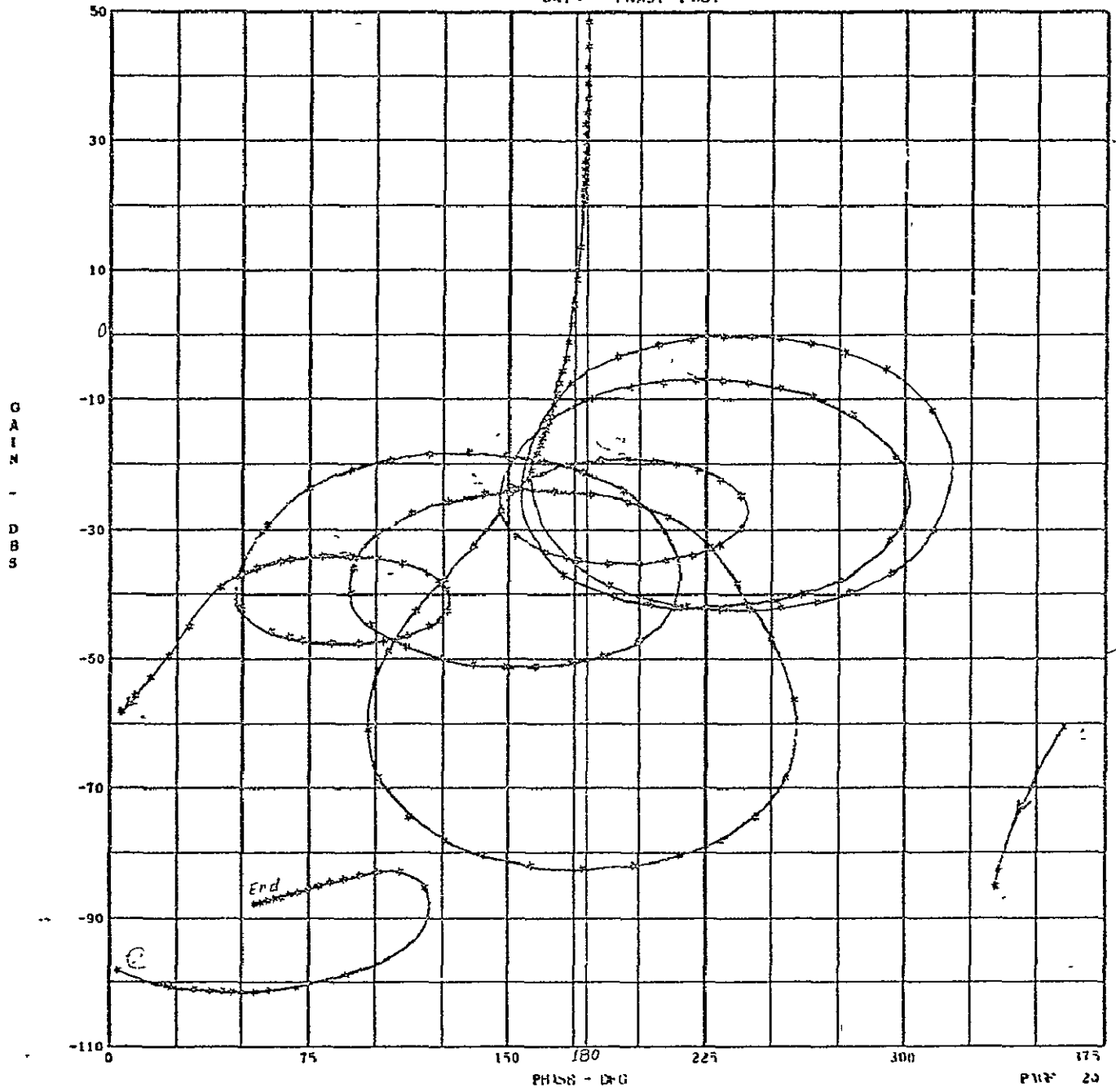


Figure 18
W PLANE FREQUENCY RESPONSE OF THE
UNCOMPENSATED SYSTEM

JSM-104/LM-3

LOAD, YAW PLANE

GAIN - PHASE PLOT

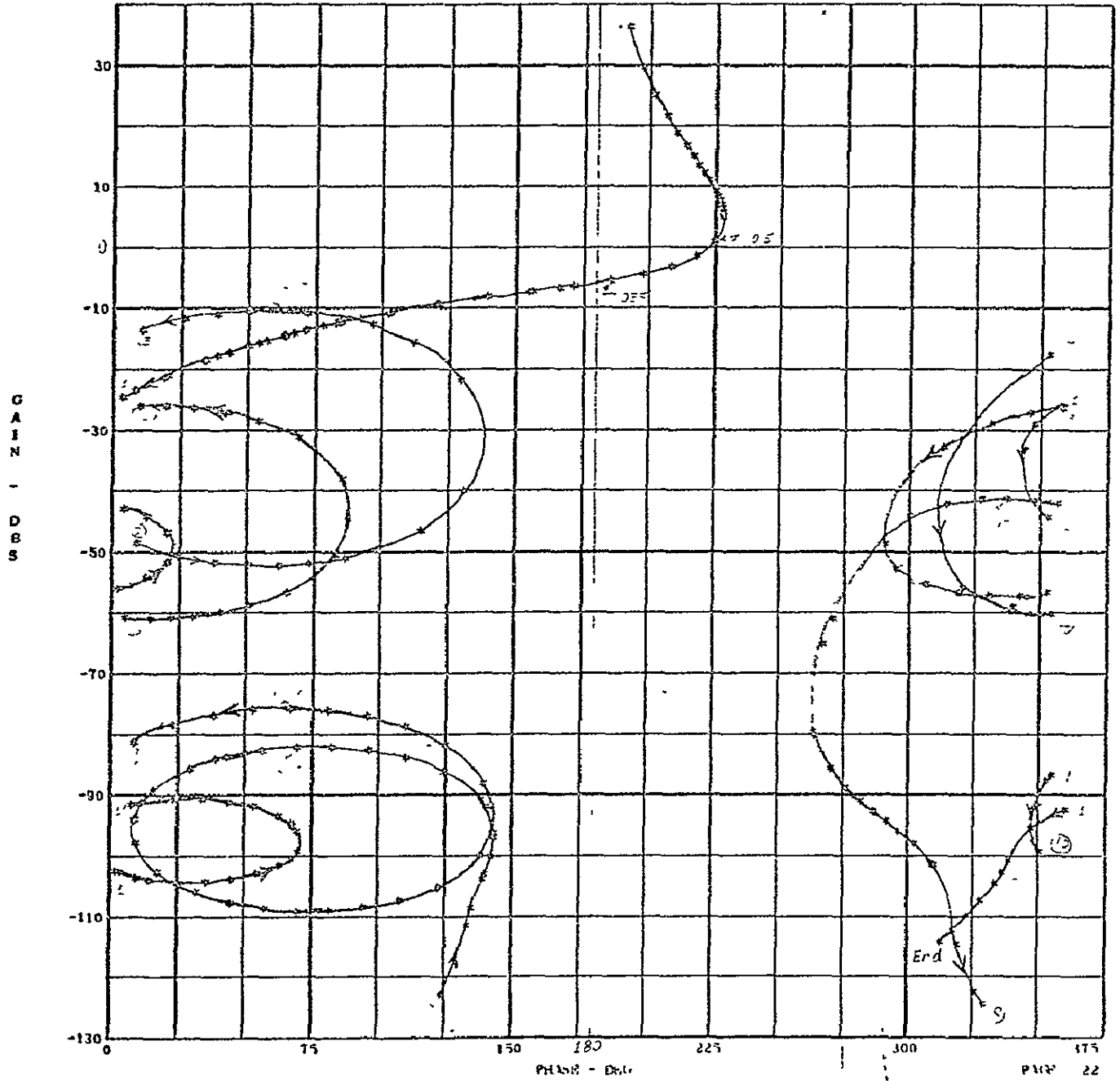


Figure 19
W-PLANE FREQUENCY RESPONSE OF THE COMPENSATED
SYSTEM USING THE DAP

CSM/19 FULL PITCH PLANE

GAIN - PHASE PLOT

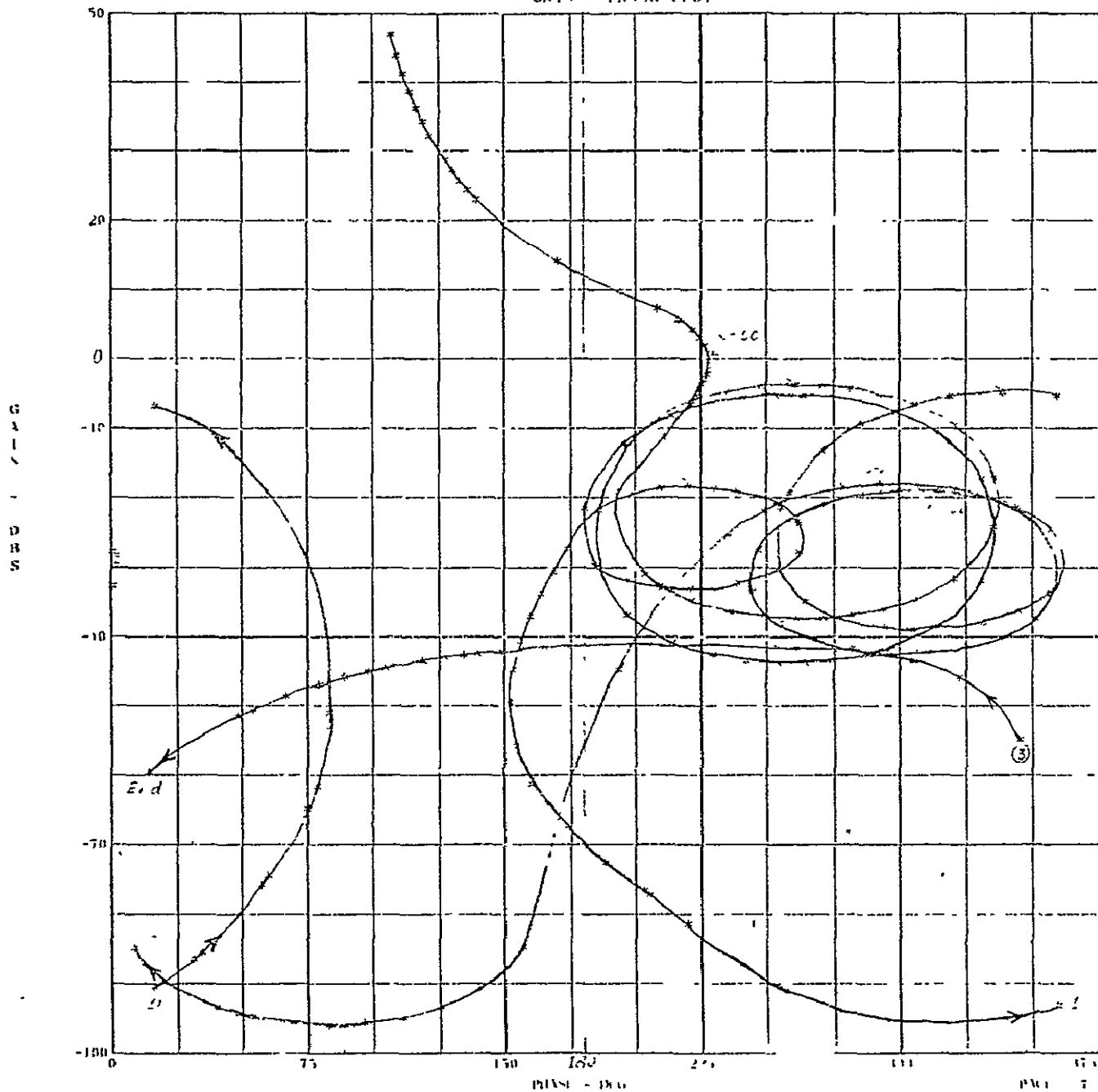


Figure 20
S-PLANE FREQUENCY RESPONSE OF THE
COMPENSATED SYSTEM USING THE SCS

CS4/14 FULL, YAW PLANE

GAIN - PHASE PLOT

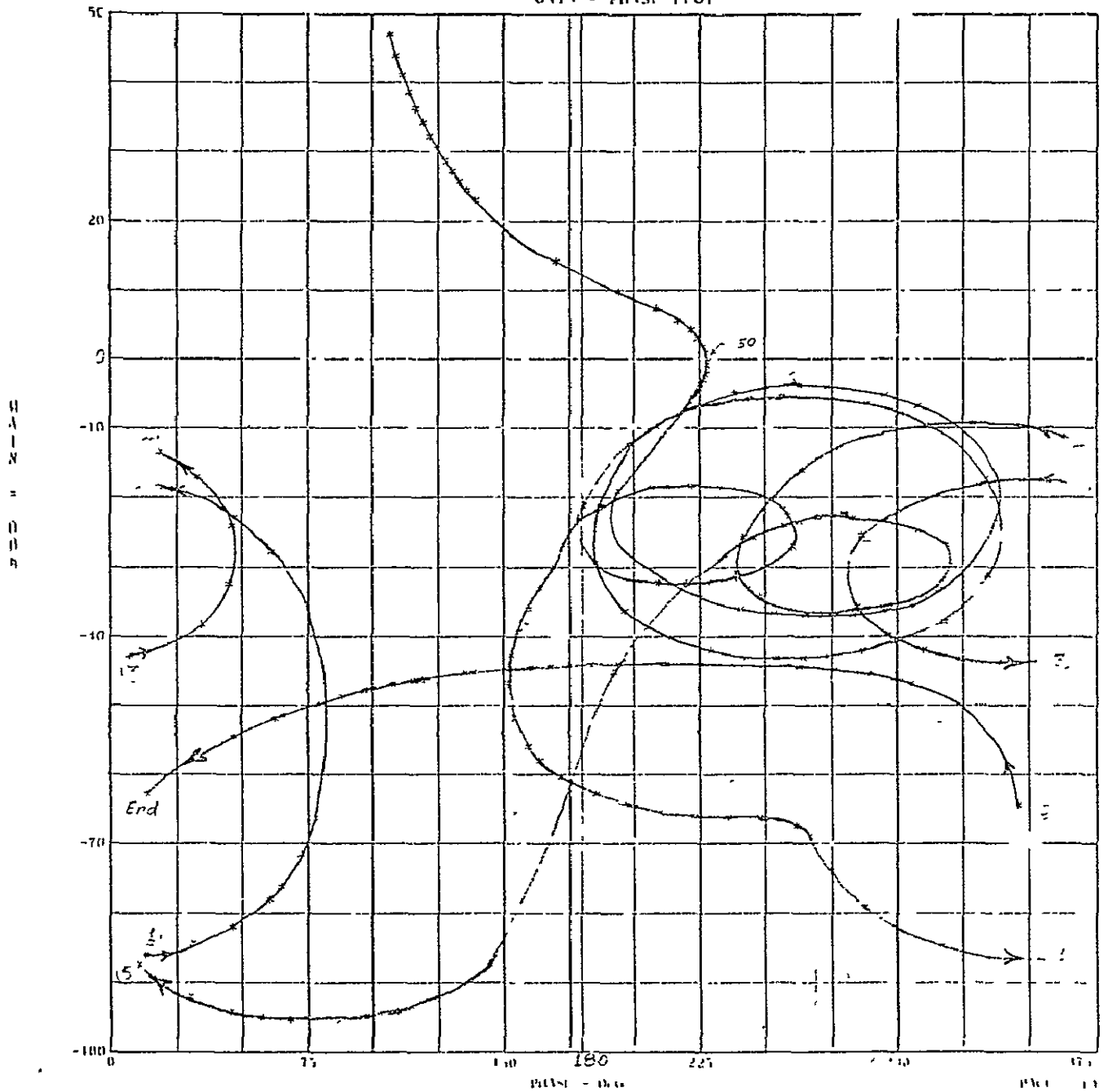


Figure 21

S-PLANE FREQUENCY RESPONSE OF THE COMPENSATED SYSTEM USING THE SCS

CSM/LM HALF FULL PITCH PLANE
GAIN - PHASE PLOT

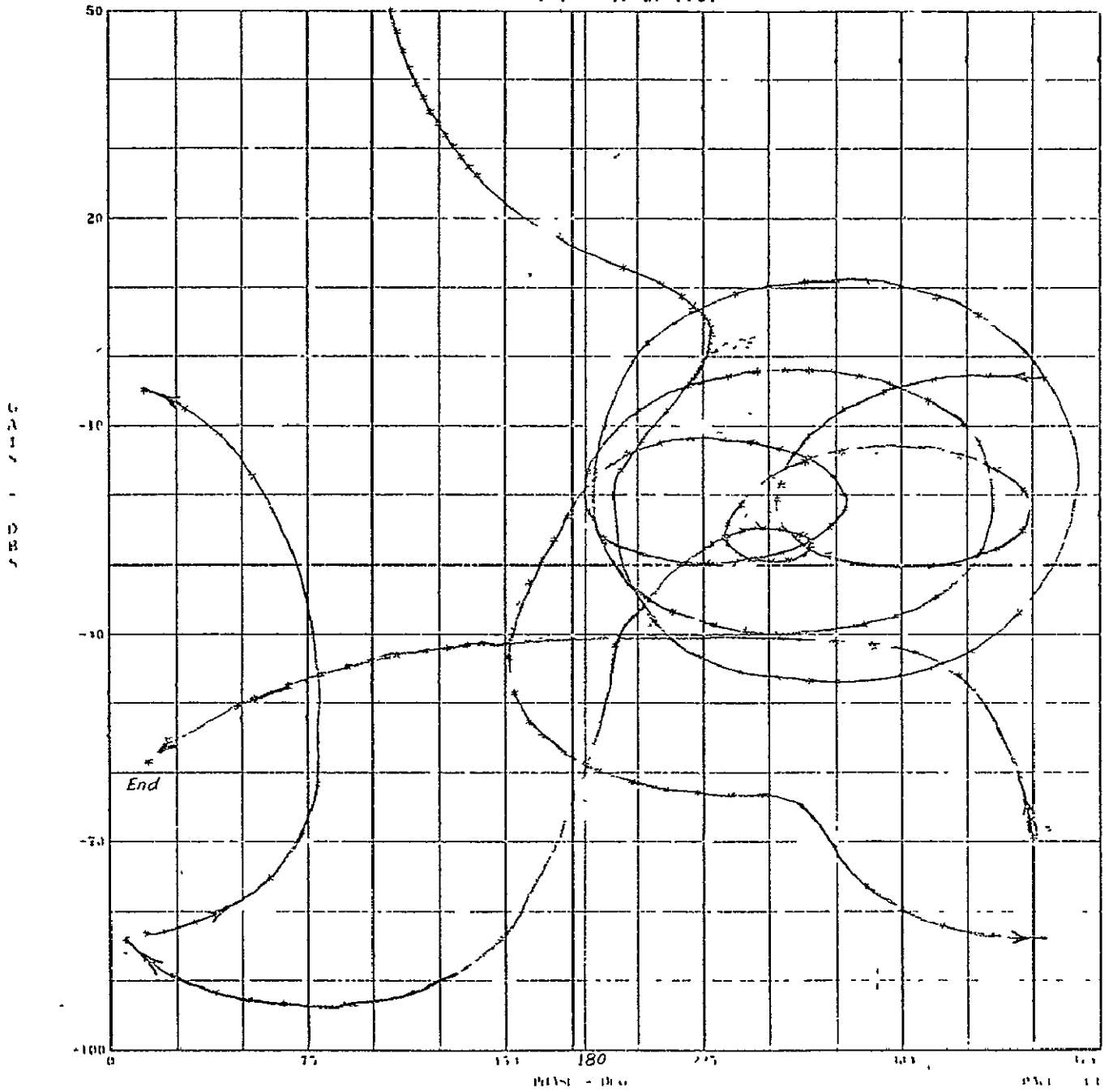


Figure 22
S-PLANE FREQUENCY RESPONSE OF THE
COMPENSATED SYSTEM USING THE SCS

CS47LM HALF FULL, YAW PLANE

GAIN - PHASE PLOT

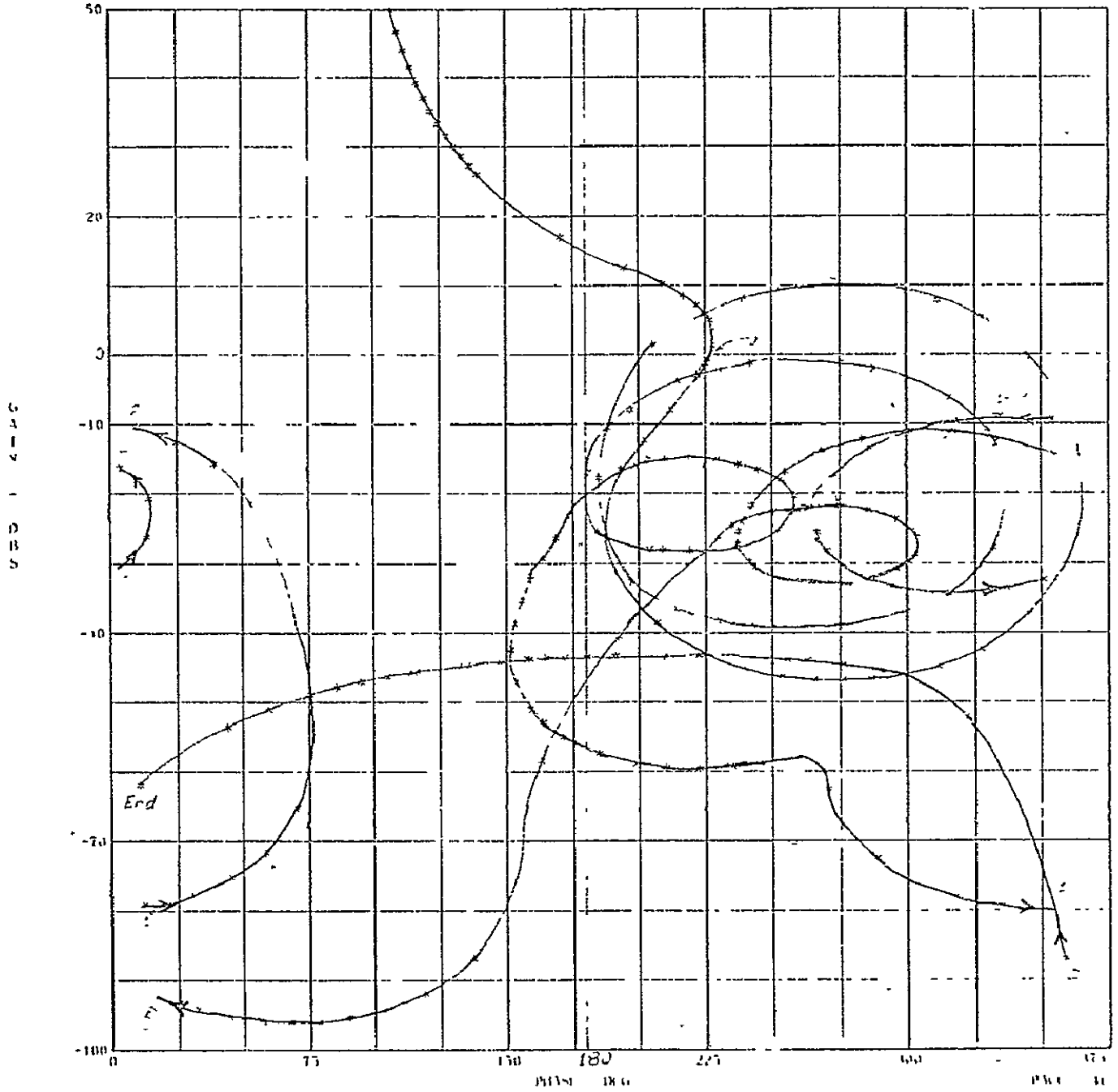


Figure 23

S-PLANE FREQUENCY RESPONSE OF THE COMPENSATED SYSTEM USING THE SCS

CSM/14 QUARTER LOAD, PITCH PLANE
GAIN - PHASE PLOT

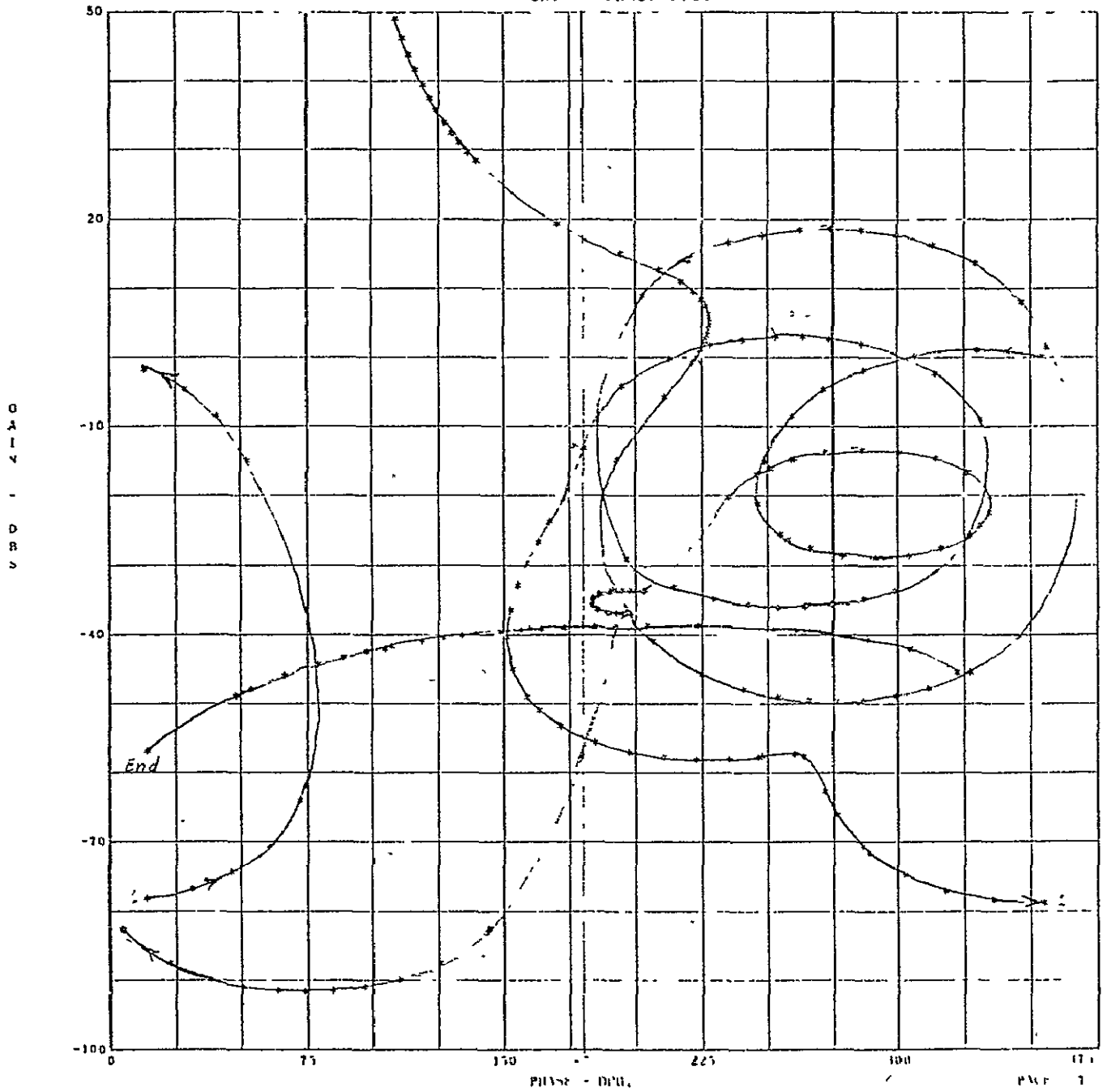


Figure 24

S-PLANE FREQUENCY RESPONSE OF THE
COMPENSATED SYSTEM USING THE SCS

CASUALTY FUEL, YAW PLANE

GAIN - PHASE PLOT

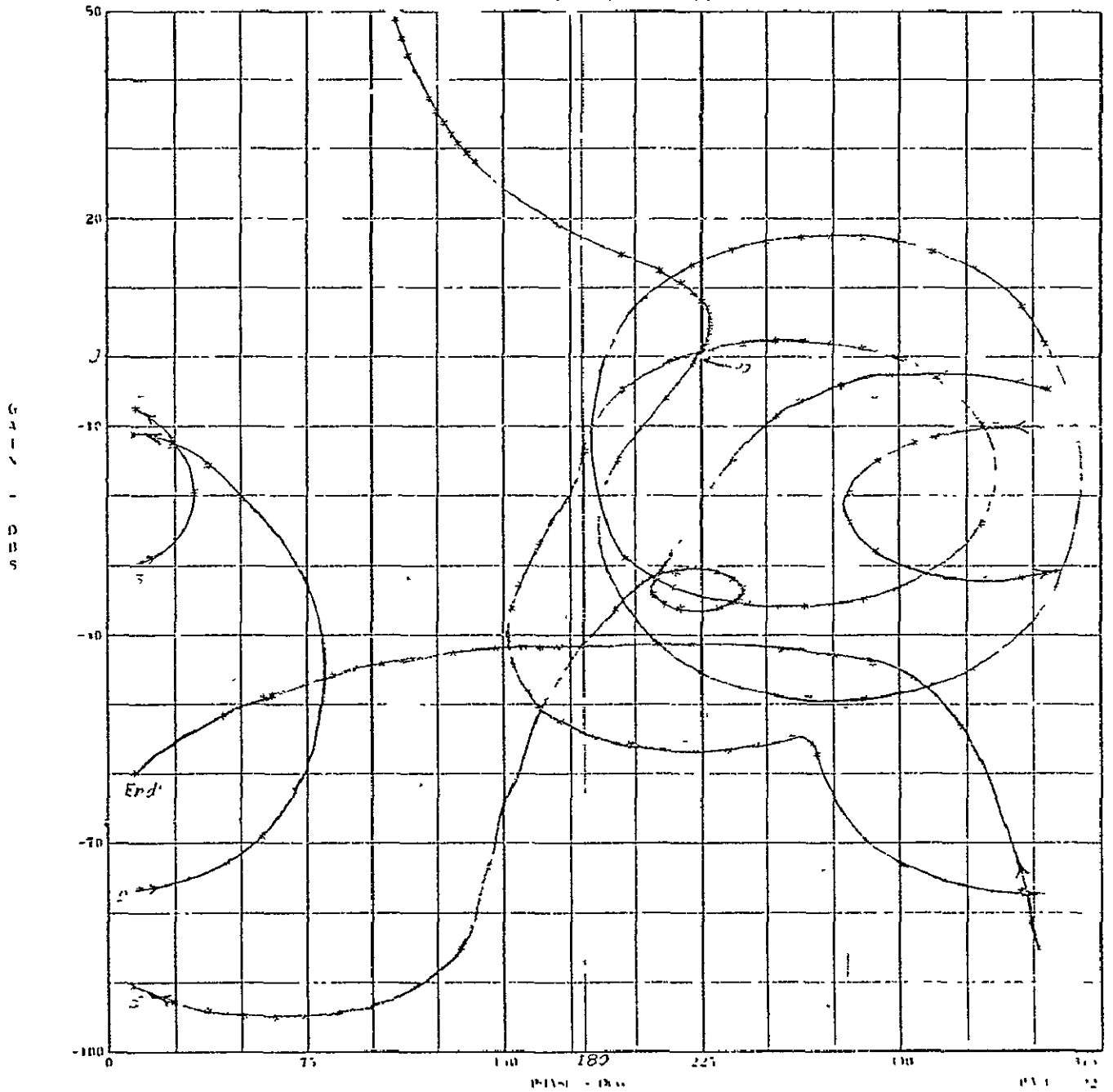


Figure 25

S-PLANE FREQUENCY RESPONSE OF THE
COMPENSATED SYSTEM USING THE SCS

CSM-10⁴/LM-3

LOAD, PITCH PLANE

GAIN - PHASE PLOT

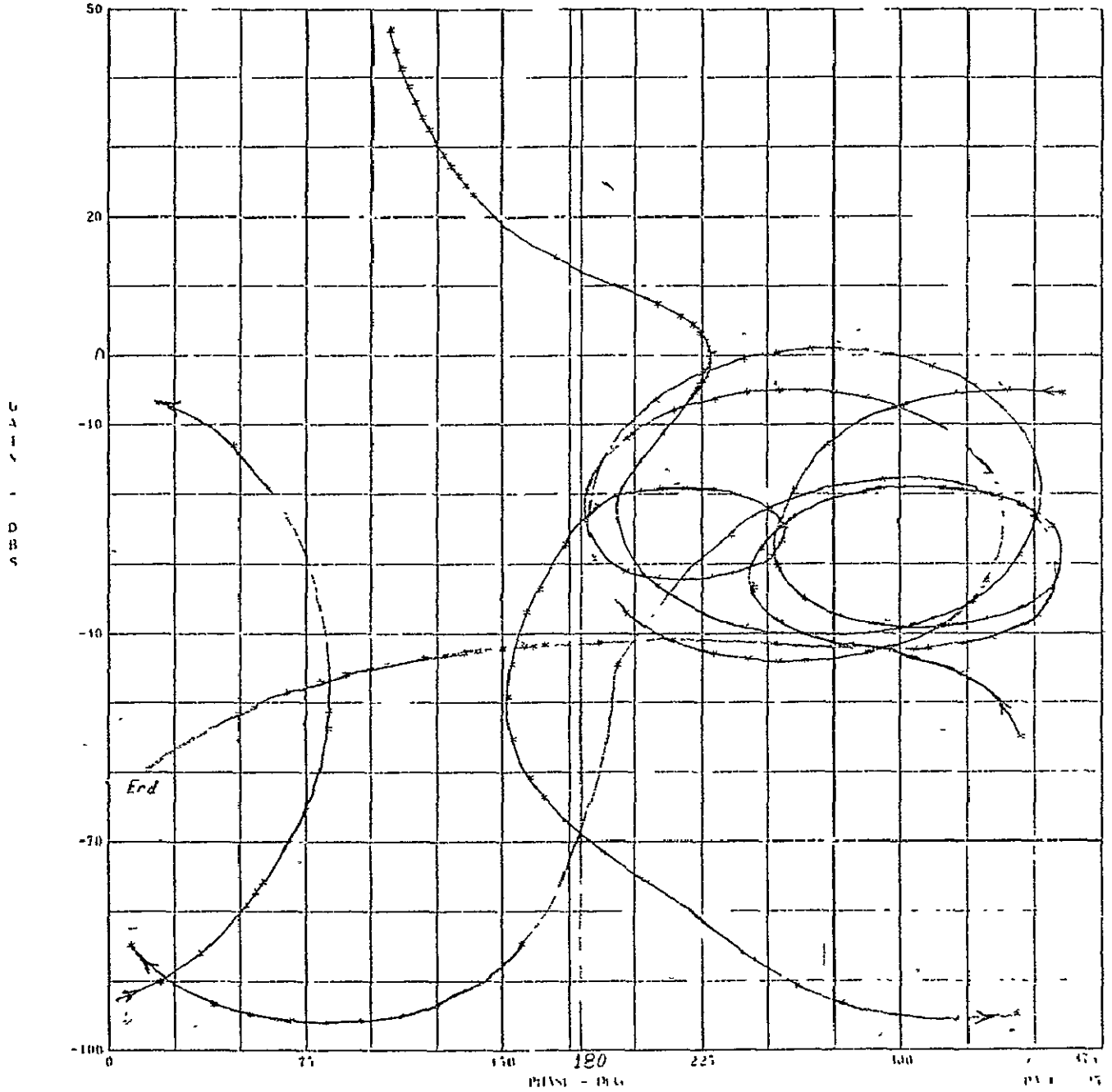


Figure 26
S-PLANE FREQUENCY RESPONSE OF THE
COMPENSATED SYSTEM USING THE SCS

CSM-10⁴/L1-3

LOAD, YAW PLANE

GAIN - PHASE PLOT

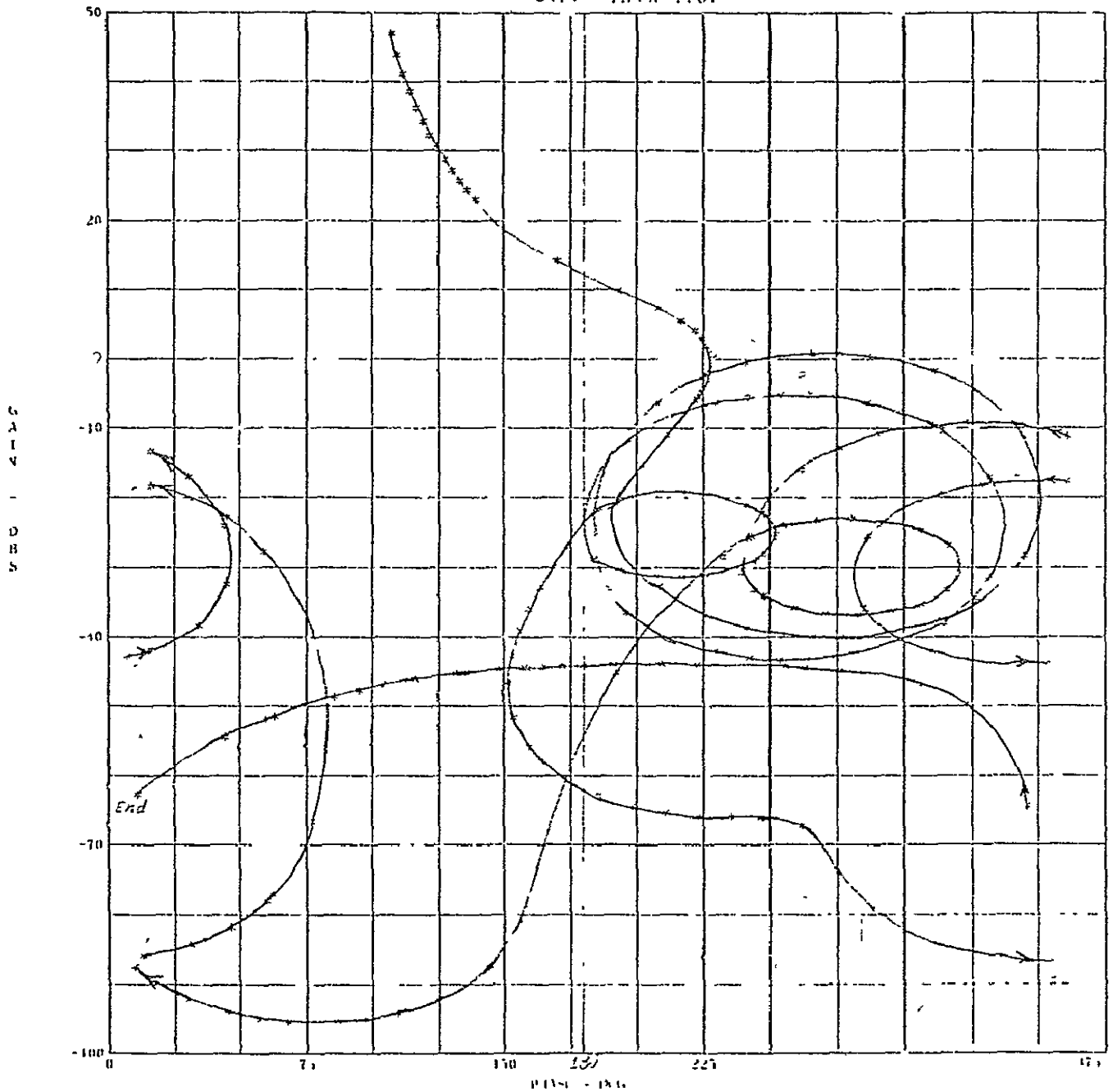


Figure 27

S-PLANE FREQUENCY RESPONSE OF THE
COMPENSATED SYSTEM USING THE SCS

CSM FULL, PITCH PLANE

GAIN - PHASE PLOT

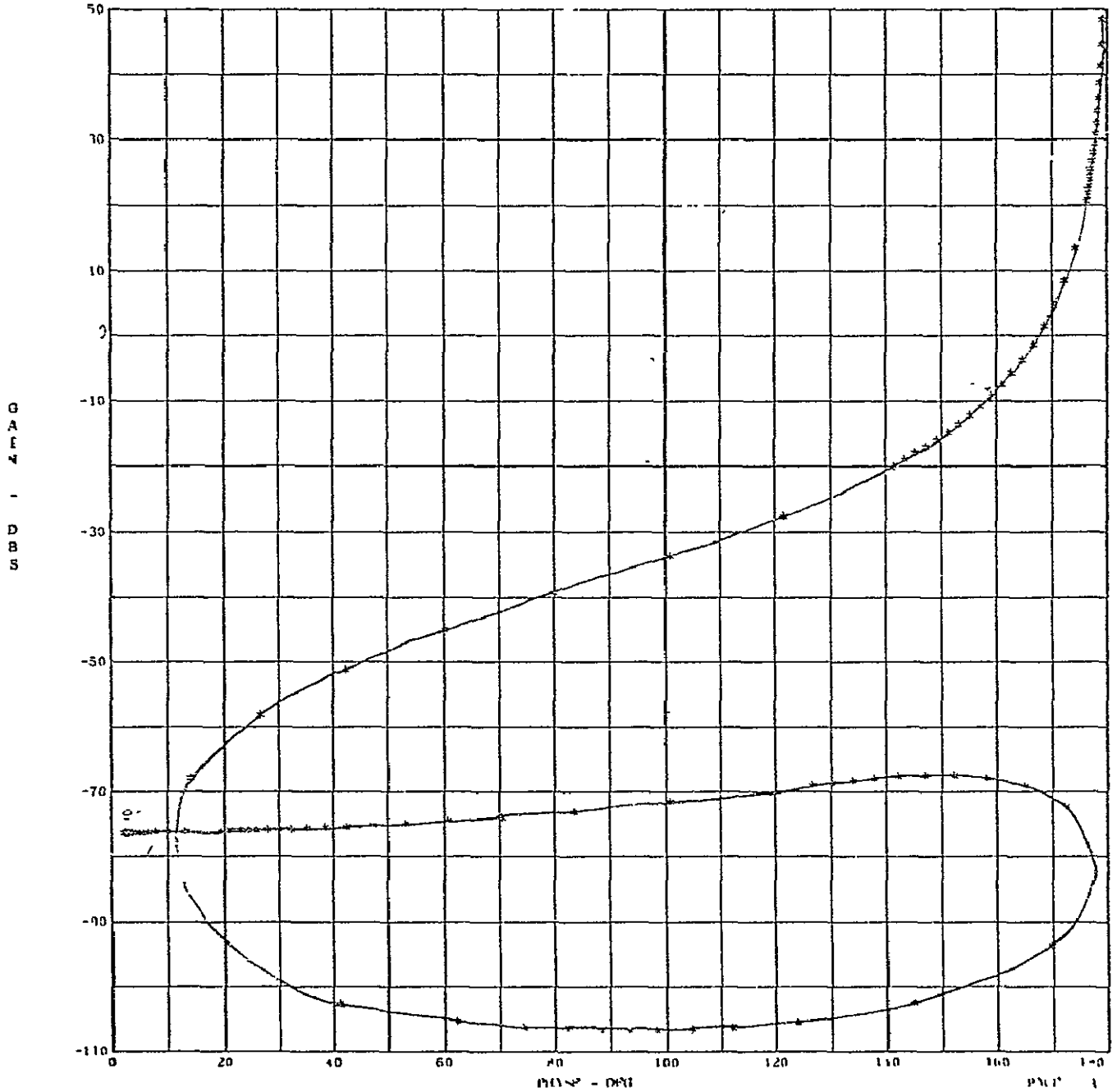


Figure 28
W-PLANE FREQUENCY RESPONSE OF THE
UNCOMPENSATED SYSTEM

CS4 FULL, PITCH PLANE

GAIN - PHASE PLOT

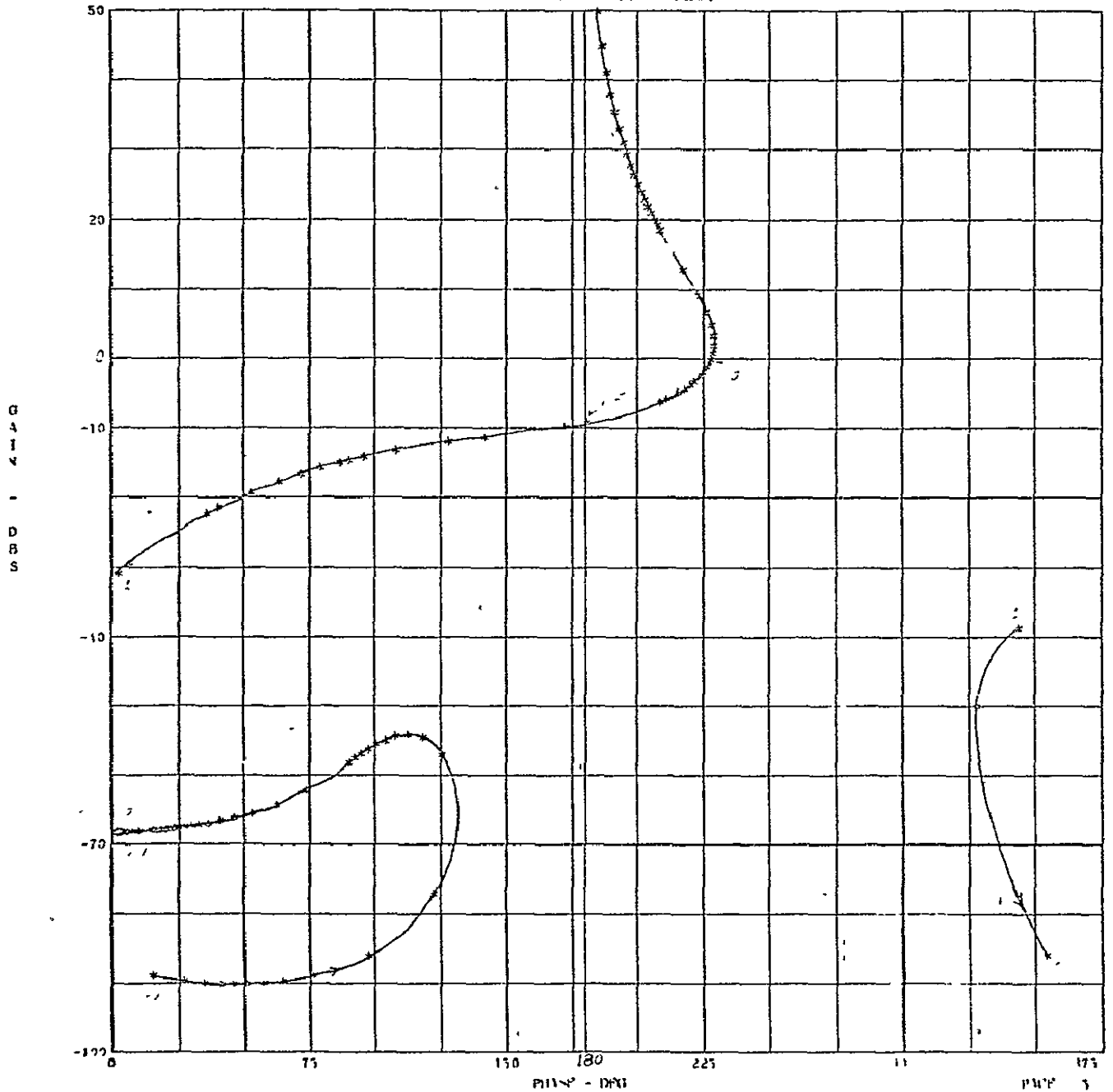


Figure 29
W-PLANE FREQUENCY RESPONSE OF THE
COMPENSATED SYSTEM USING THE DAP

CSM FULL, YAW PLANE

GAIN - PHASE PLOT

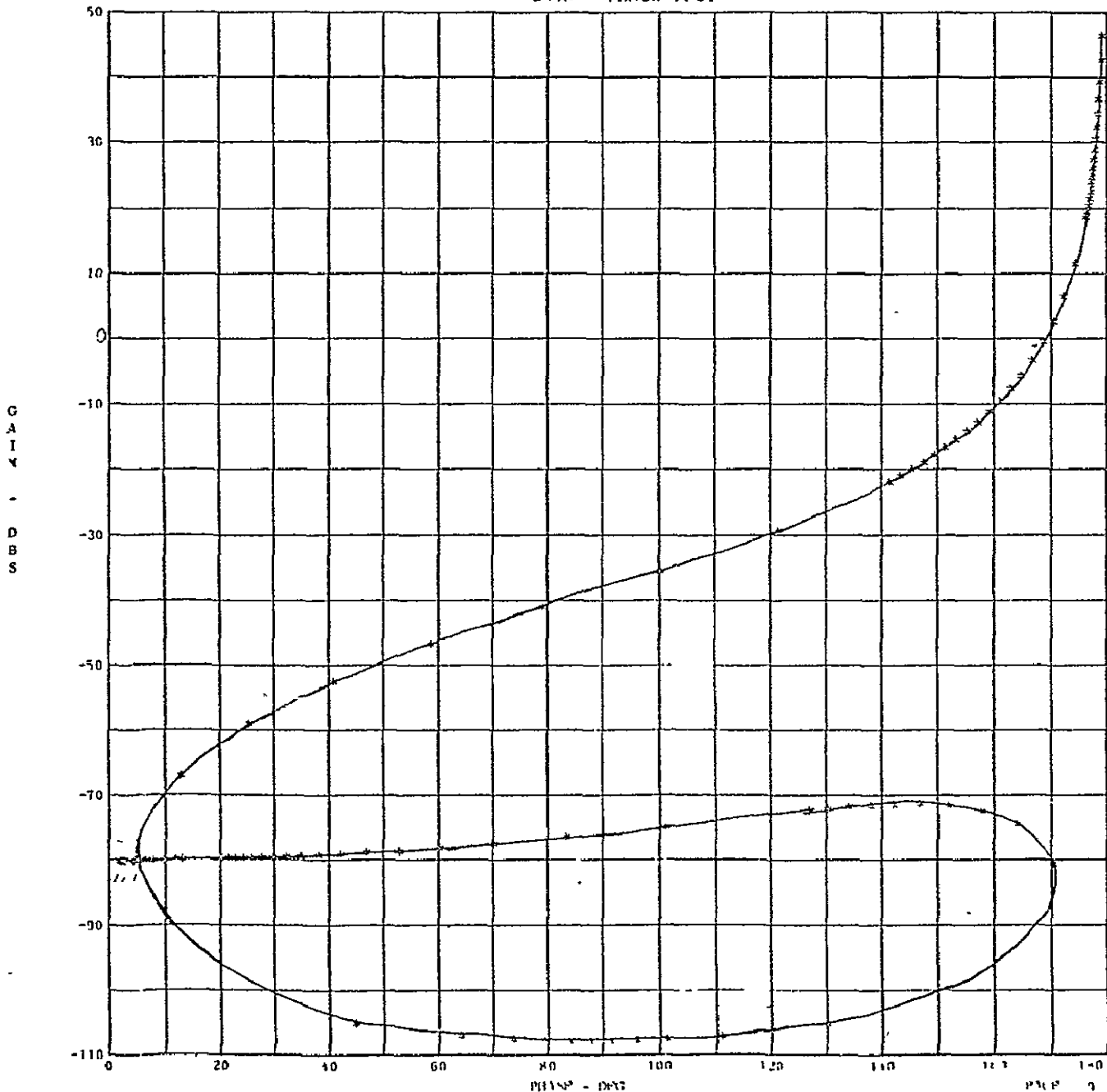


Figure 30
W-PLANE FREQUENCY RESPONSE OF THE
UNCOMPENSATED SYSTEM

CSM PULL, YAW PLANE

GAIN - PHASE PLOT

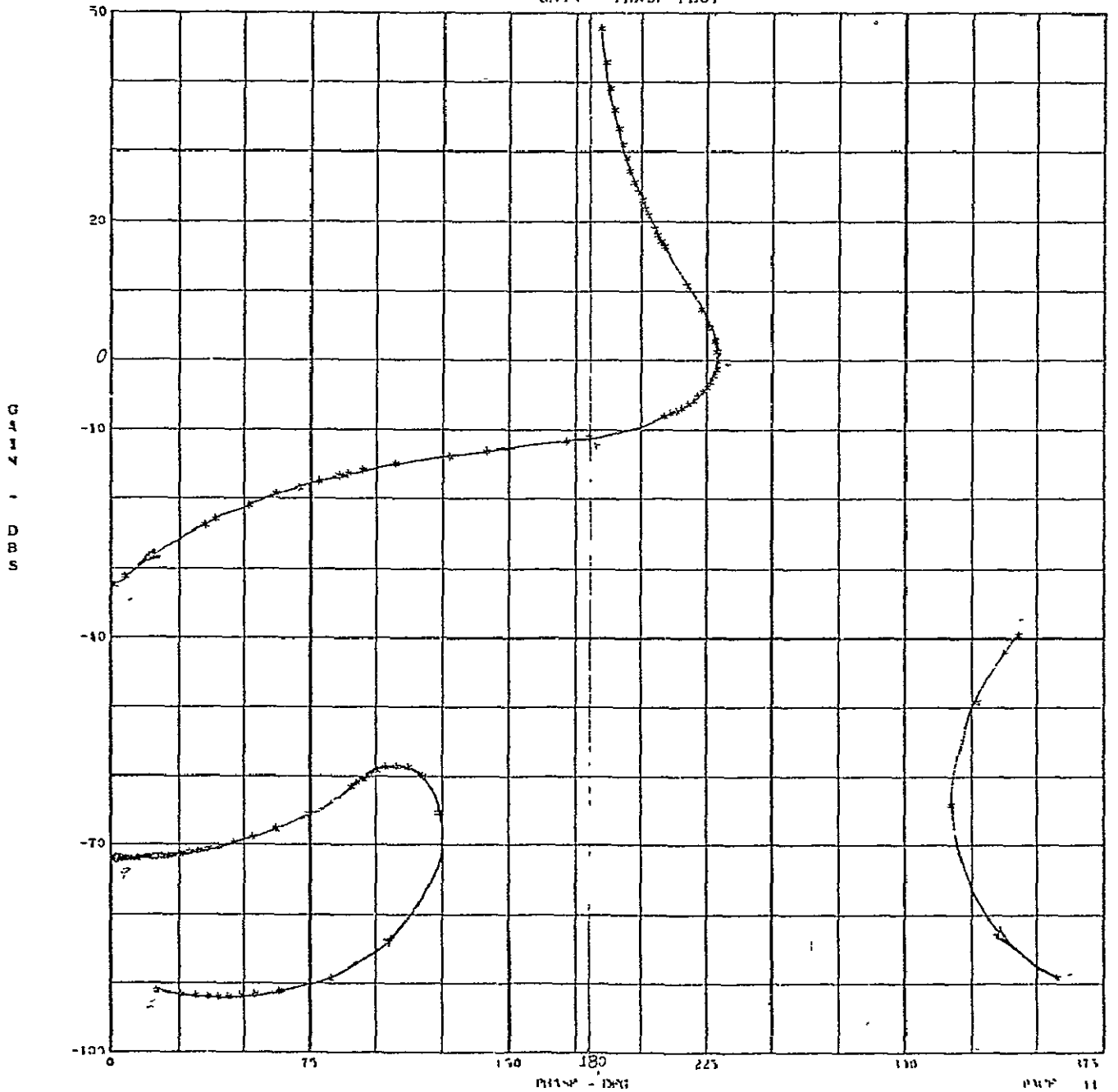


Figure 31
W-PLANE FREQUENCY RESPONSE OF THE
COMPENSATED SYSTEM USING THE DAP

CSM HALF-PULL, PITCH PLANE

GAIN - PHASE PLOT

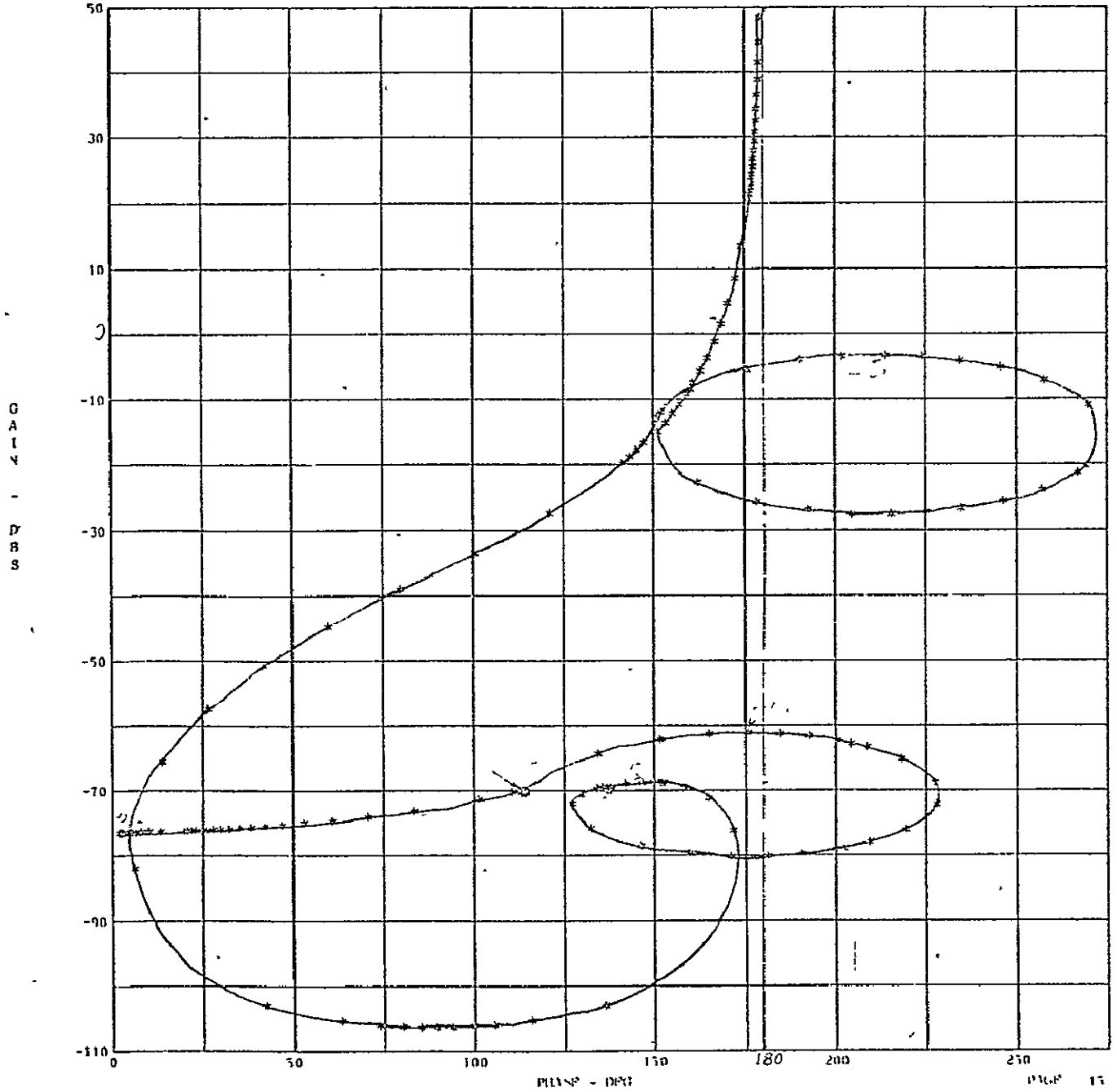


Figure 32
W-PLANE FREQUENCY RESPONSE OF THE
UNCOMPENSATED SYSTEM

CS4 HALF-FULL, PITCH PLANE

GAIN - PHASE PLOT

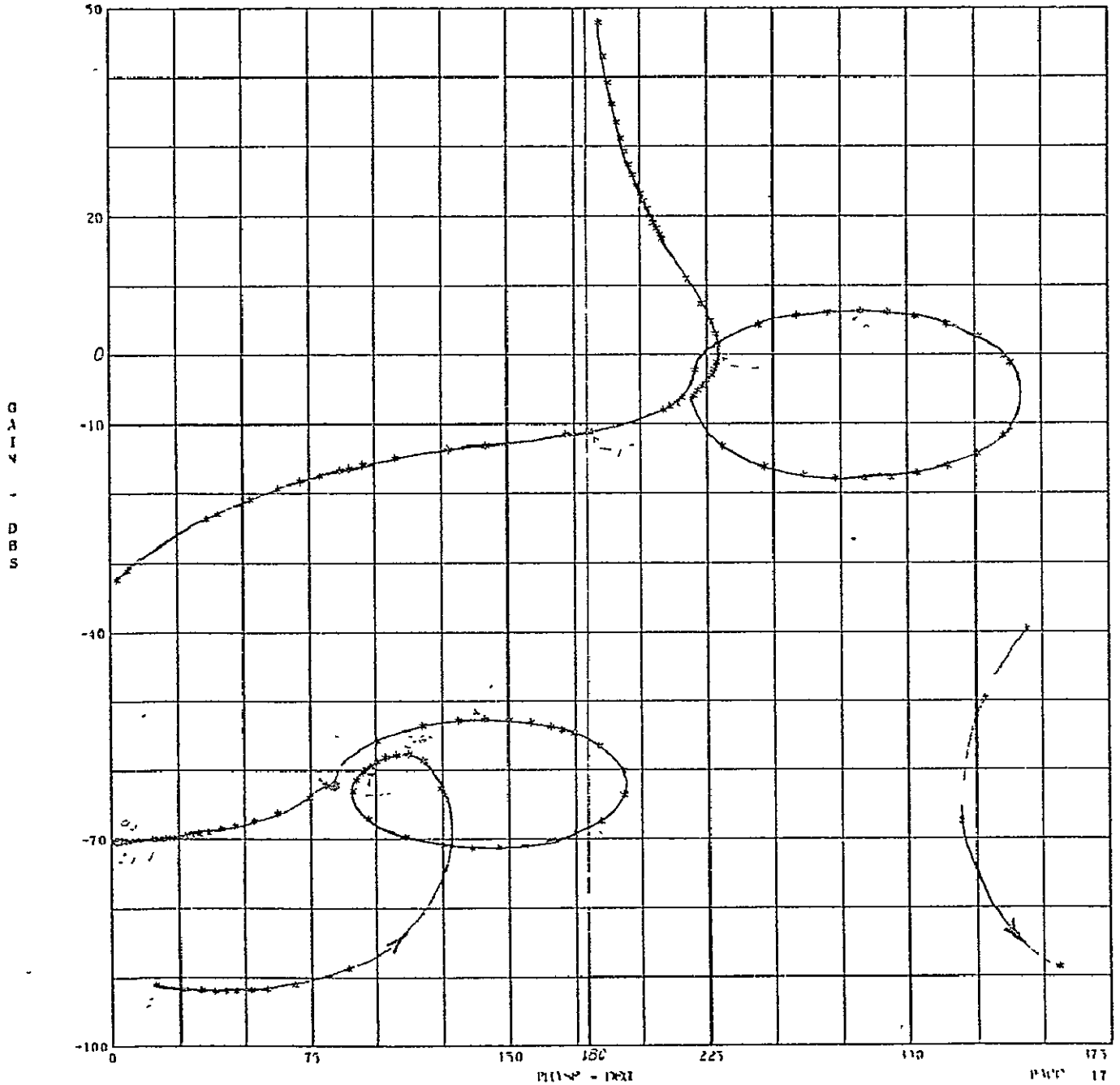


Figure 33
W-PLANE FREQUENCY RESPONSE OF THE
COMPENSATED SYSTEM USING THE DA?

CSM HALF-PULL, YAW PLANE

GAIN - PHASE PLOT

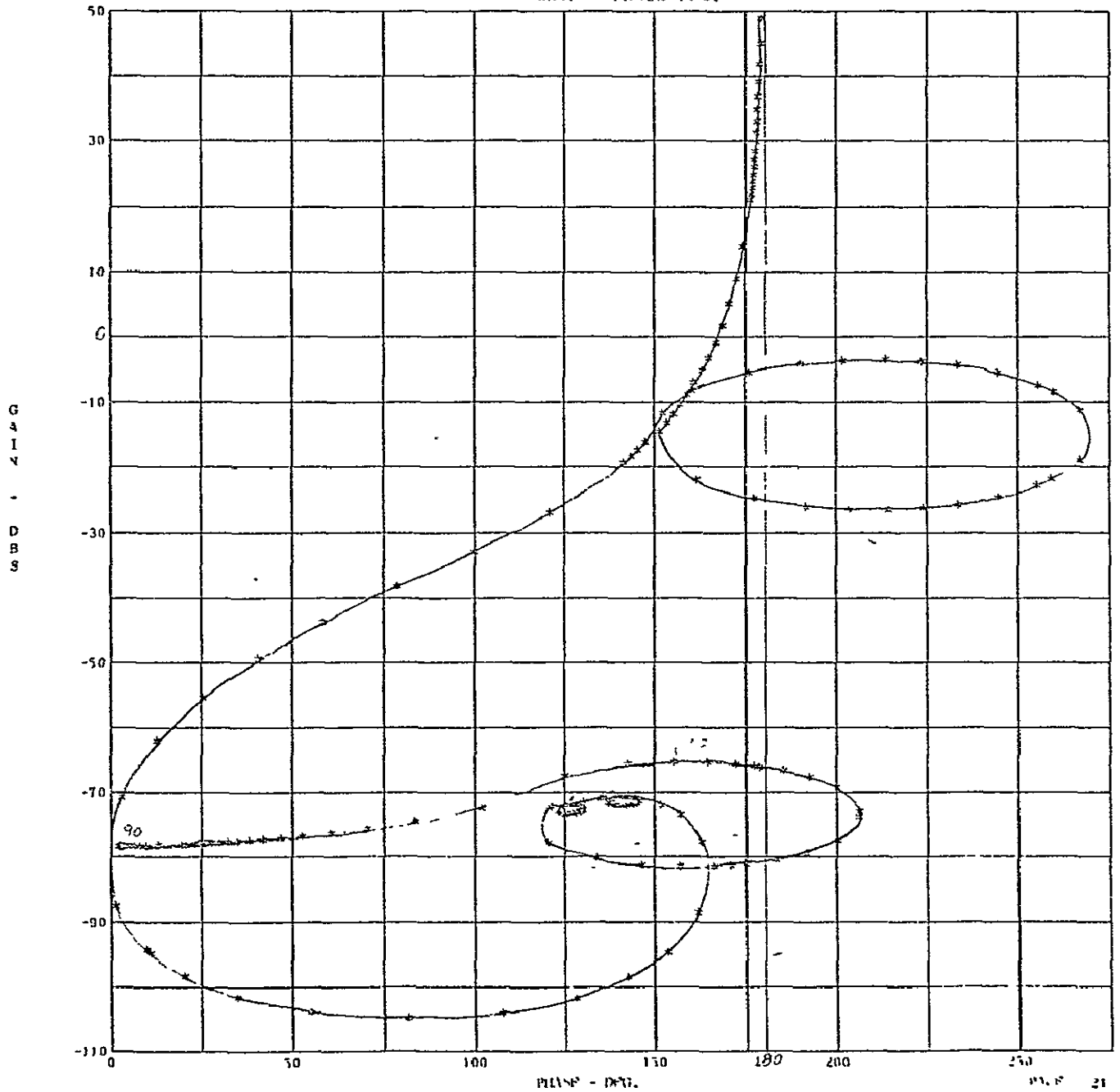


Figure 34
W-PLANE FREQUENCY RESPONSE OF THE
UNCOMPENSATED SYSTEM

CSM HALP-PULL, YAW PLANE

GAIN - PHASE PLOT

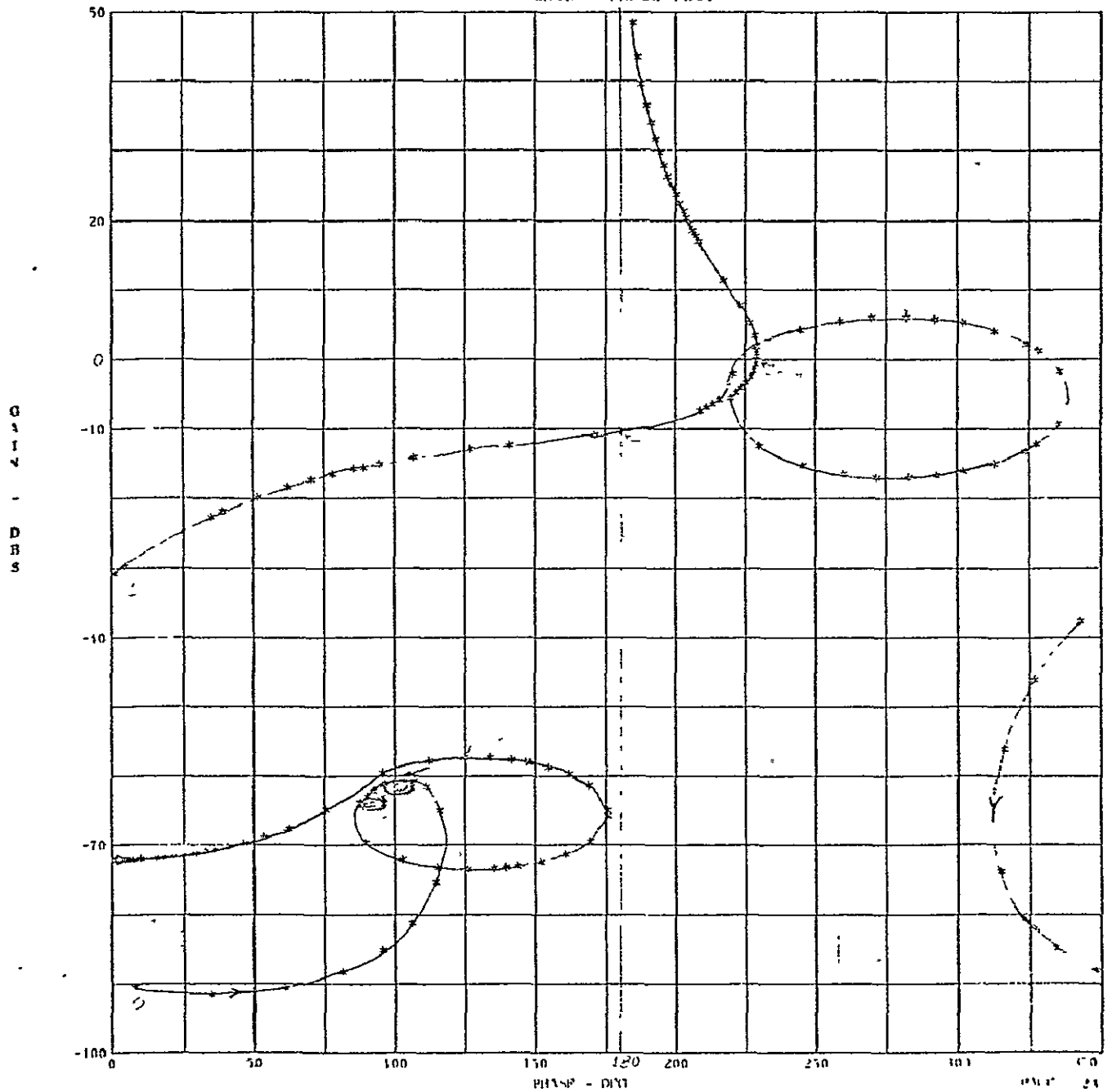


Figure 35
W-PLANE FREQUENCY RESPONSE OF THE
COMPENSATED SYSTEM USING THE DAP

C94 QUARTER PULL, PITCH PLANE

GAIN - PHASE PLOT

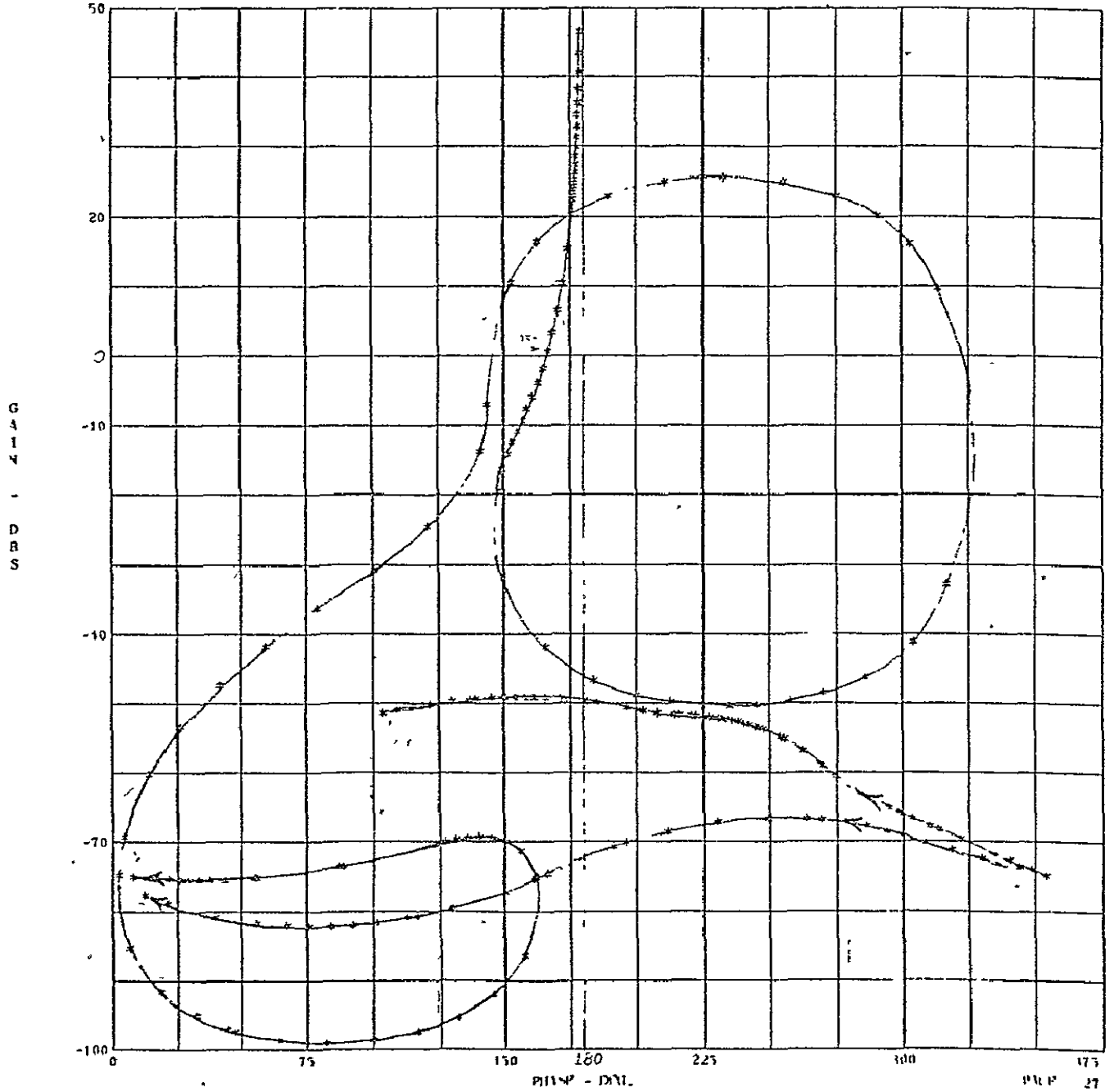


Figure 36
W-PLANE FREQUENCY RESPONSE OF THE
UNCOMPENSATED SYSTEM

CSM QUARTER FULL, PITCH PLANE

GAIN - PHASE PLOT

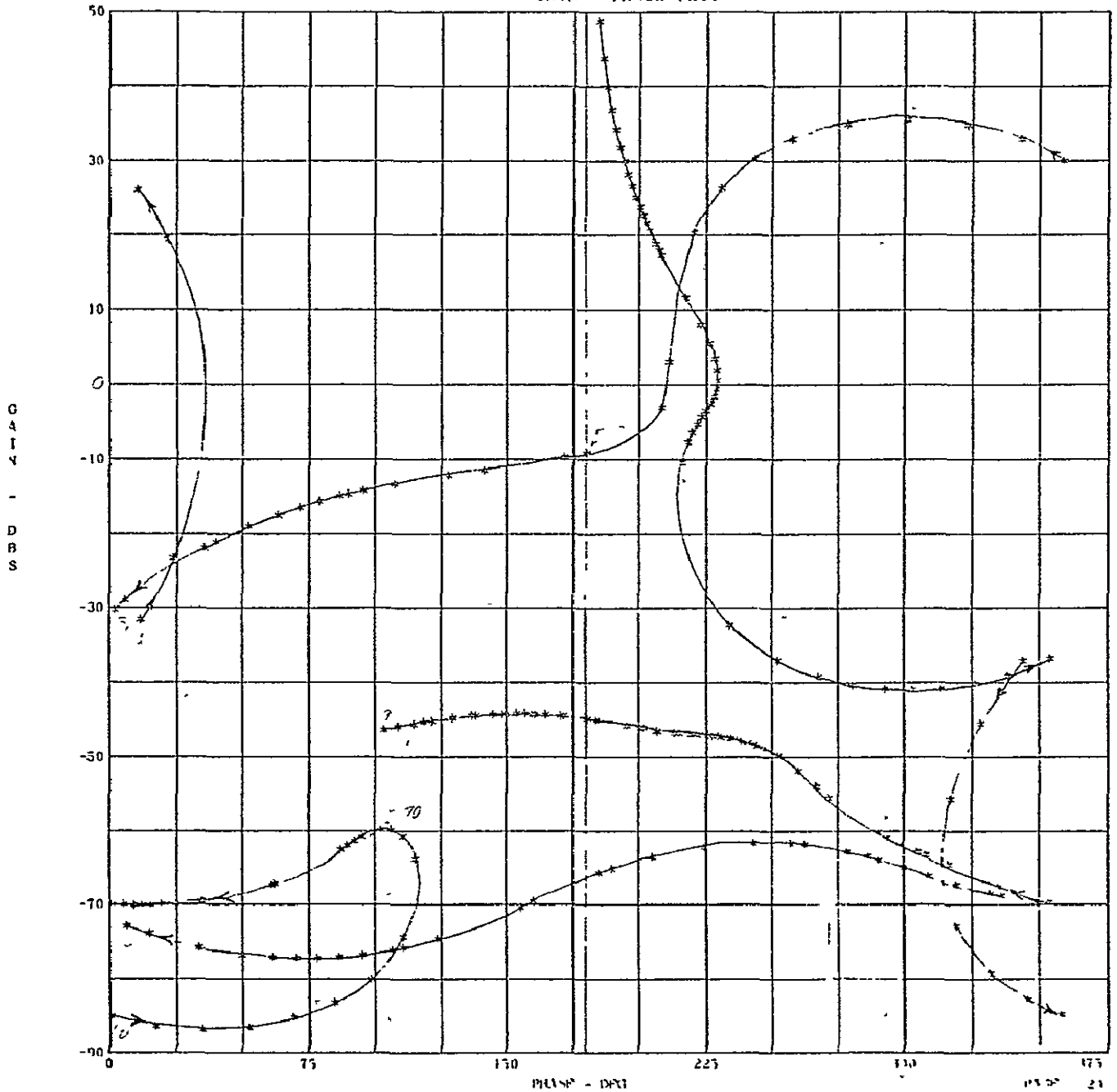


Figure 37
W-PLANE FREQUENCY RESPONSE OF THE
COMPENSATED SYSTEM USING THE DAP

CSM QUARTER FULL, YAW PLANE

GAIN - PHASE PLOT

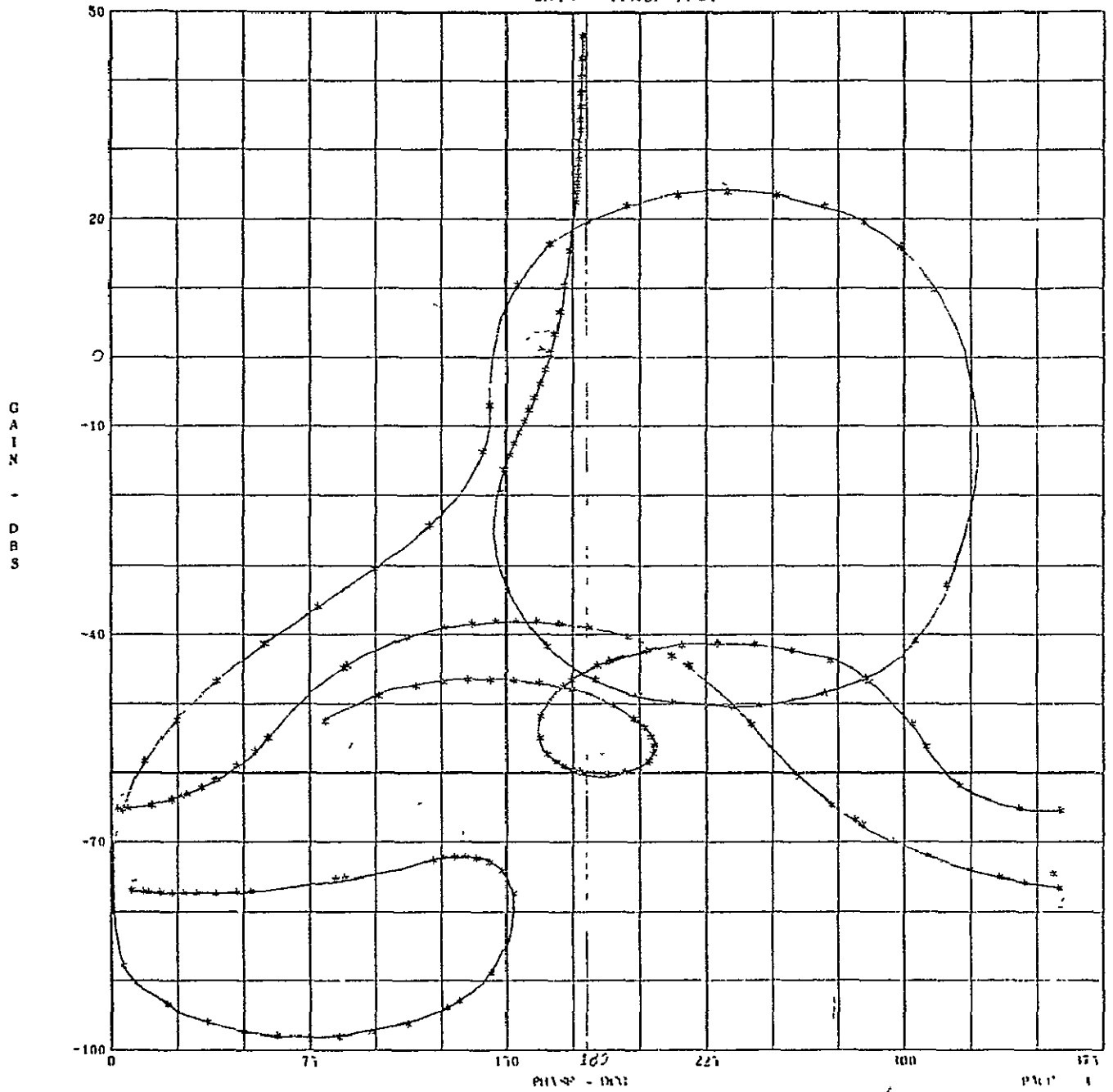


Figure 38
W-PLANE FREQUENCY RESPONSE OF THE
UNCOMPENSATED SYSTEM

CSM QUARTER PULL, YAW PLANE

GAIN - PHASE PLOT

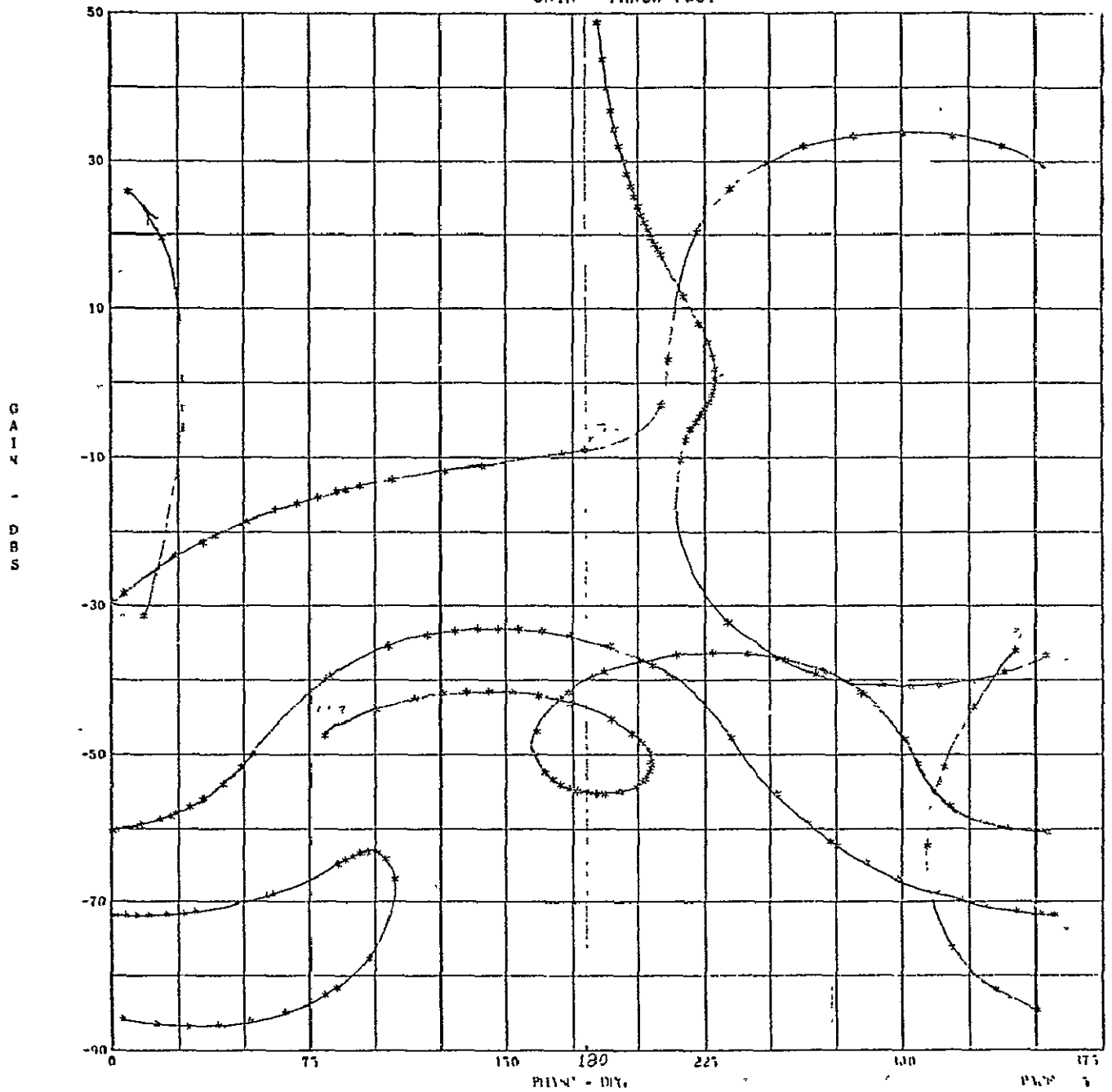


Figure 39
W-PLANE FREQUENCY RESPONSE OF THE
COMPENSATED SYSTEM USING THE DAP

CSS POL, PITCH PLANE

GAIN - PHASE PLOT

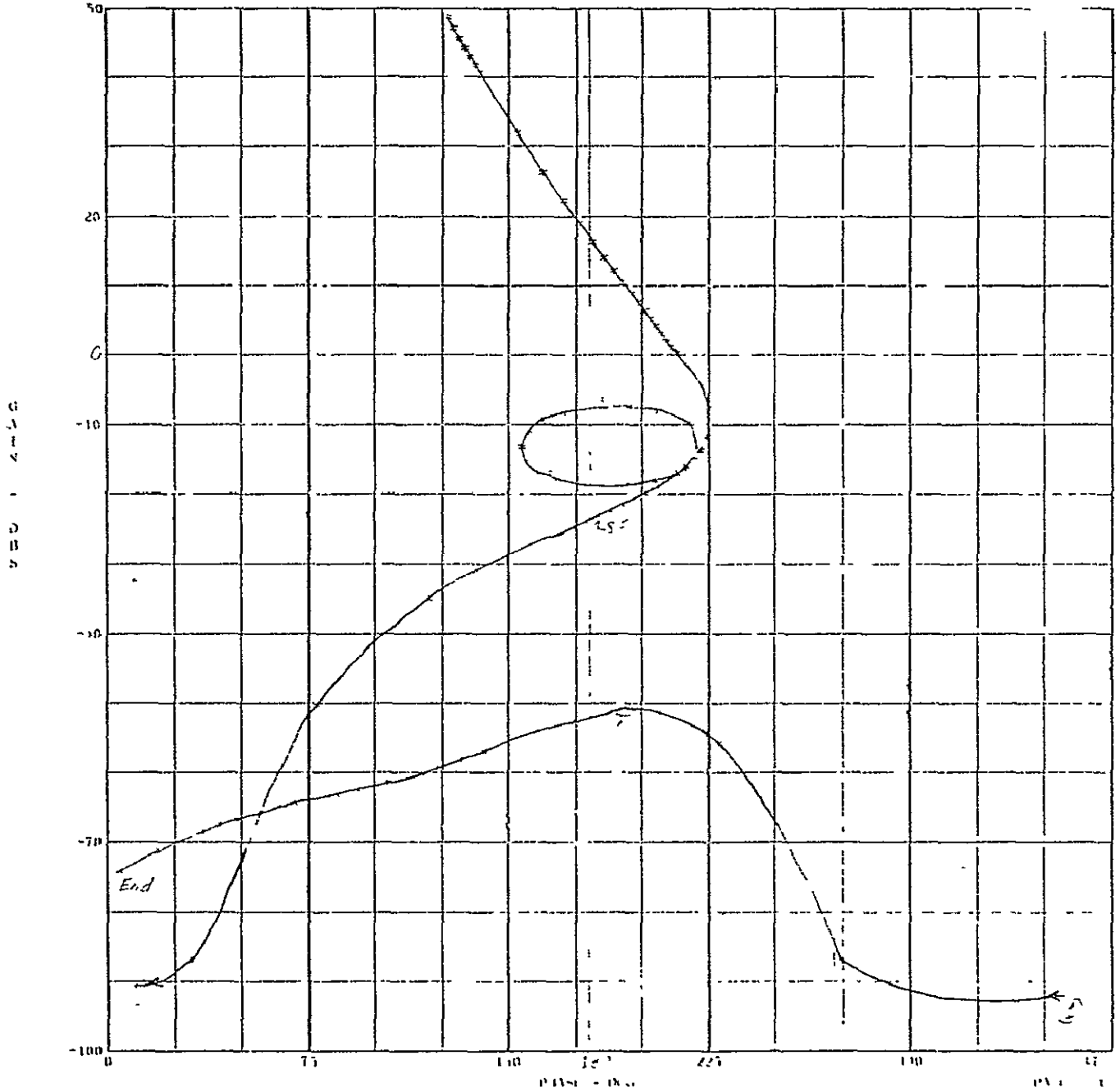


Figure 40
S-PLANE FREQUENCY RESPONSE OF THE
COMPENSATED SYSTEM USING THE GCS

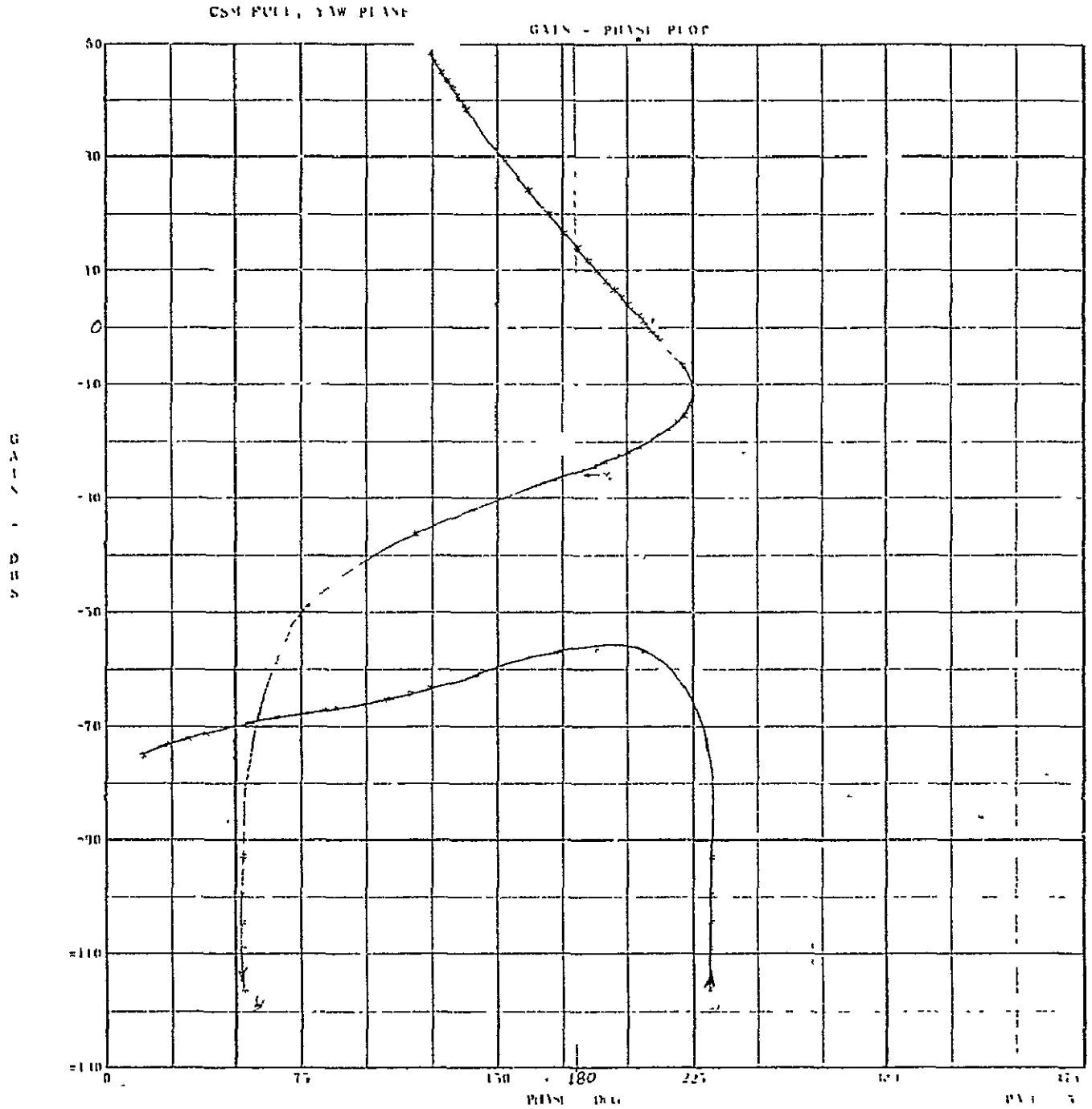


Figure 41
S-PLANE FREQUENCY RESPONSE OF THE
COMPENSATED SYSTEM USING THE SCS

CSM HALF-FULL, PITCH PLANT

GAIN - PHASE PLOT

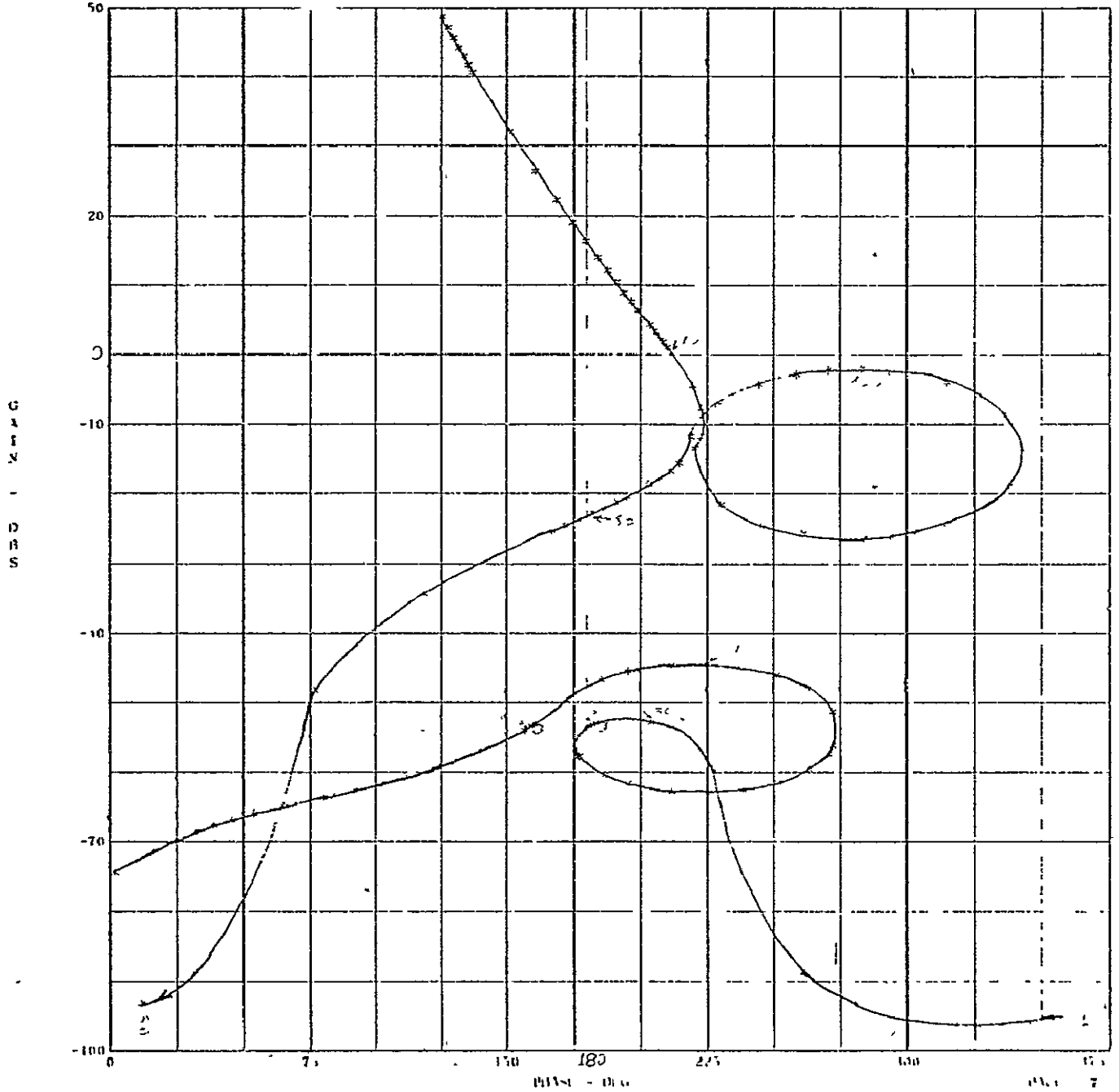


Figure 42
S-PLANE FREQUENCY RESPONSE OF THE
COMPENSATED SYSTEM USING THE SCS

CSM HALF-FULL, YAW PLANE

GAIN - PHASE PLOT

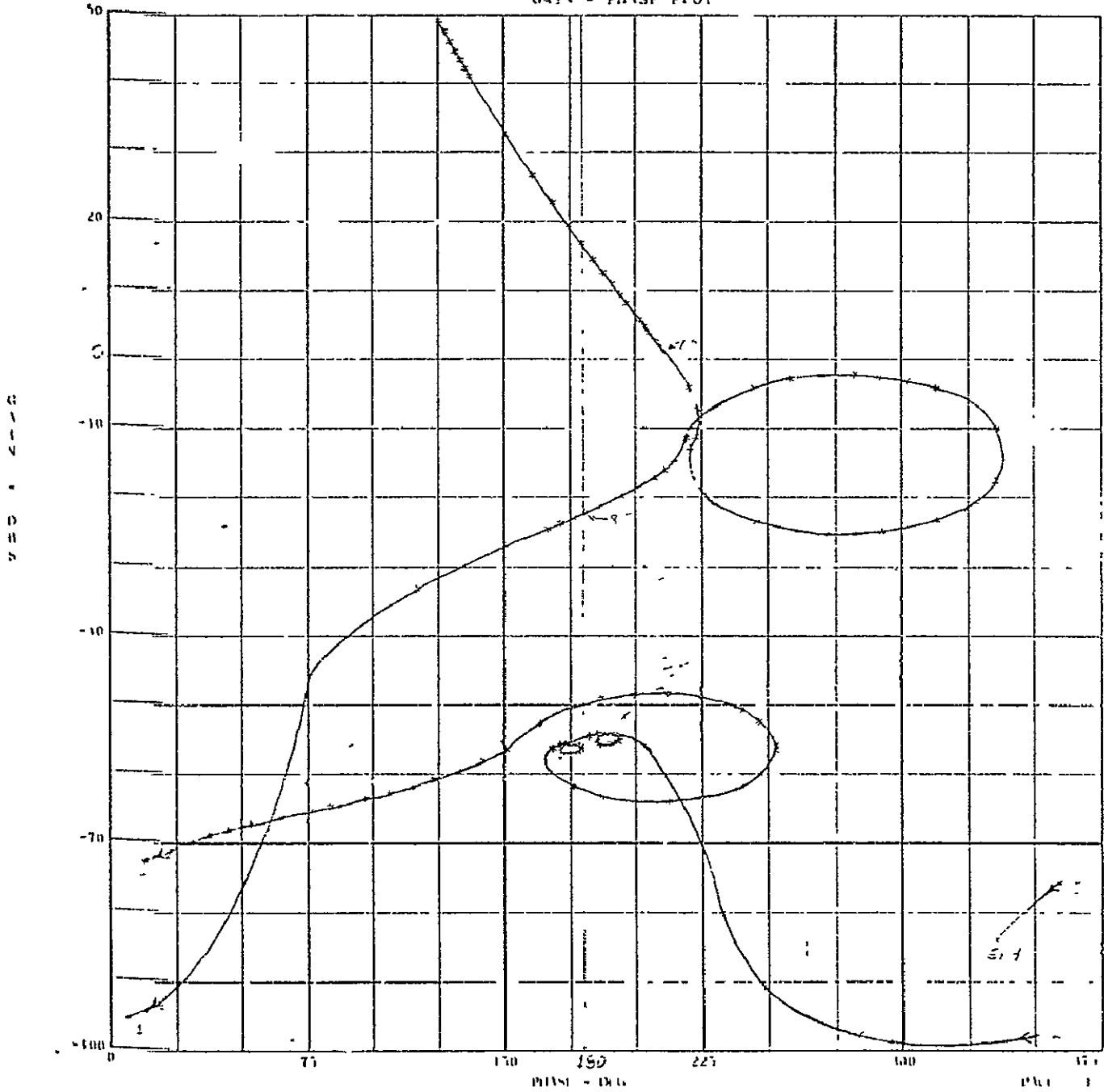


Figure 43 -
S-PLANE FREQUENCY RESPONSE OF THE
COMPENSATED SYSTEM USING THE SCS

CSM QUARTER FULL, PITCH PLANE GAIN - PHASE PLOT

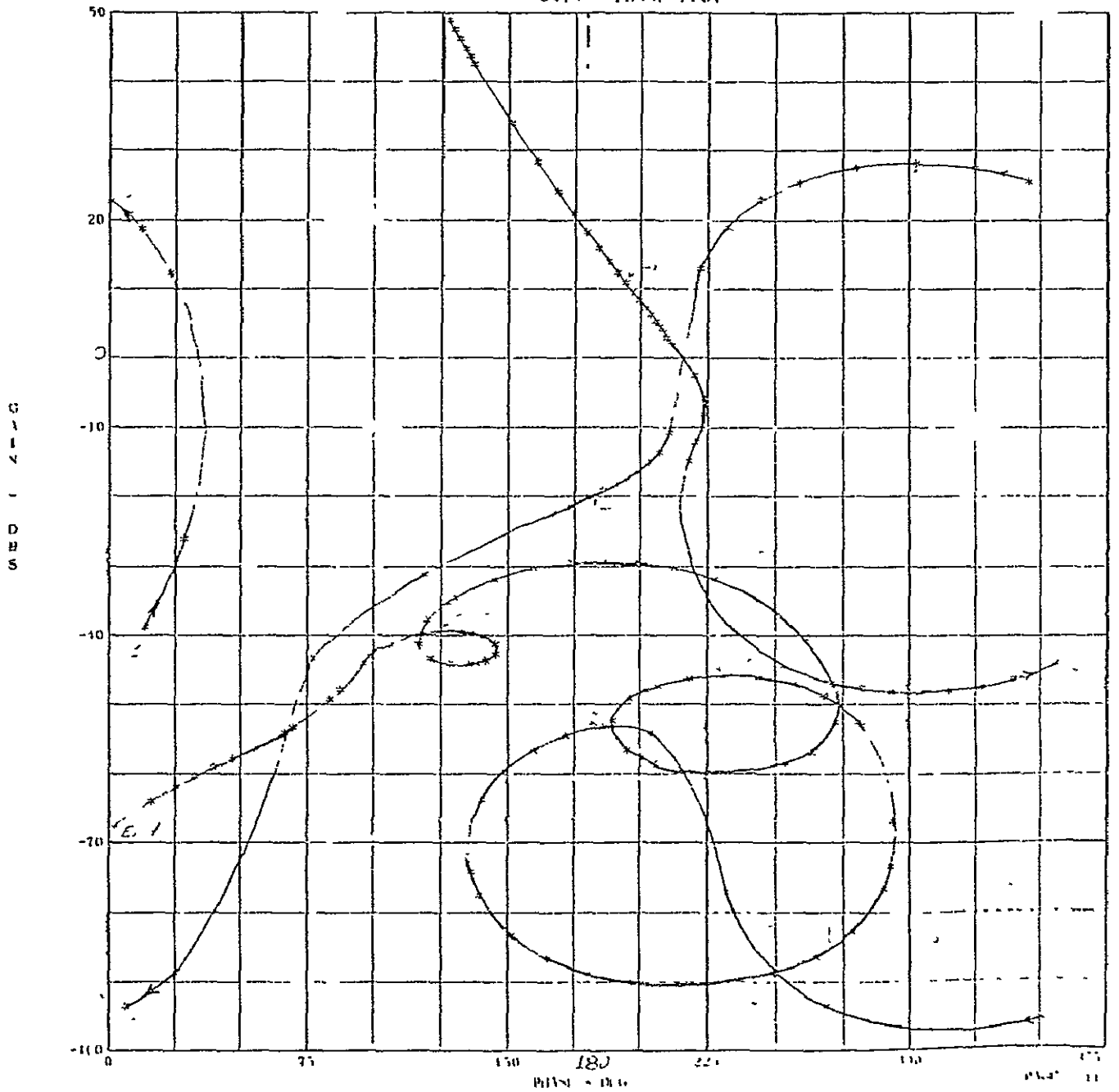


Figure 44
S-PLANE FREQUENCY RESPONSE OF THE
COMPENSATED SYSTEM USING THE SCS

CS4 QUARTER FULL, YAW PLANE

GAIN - PHASE PLOT

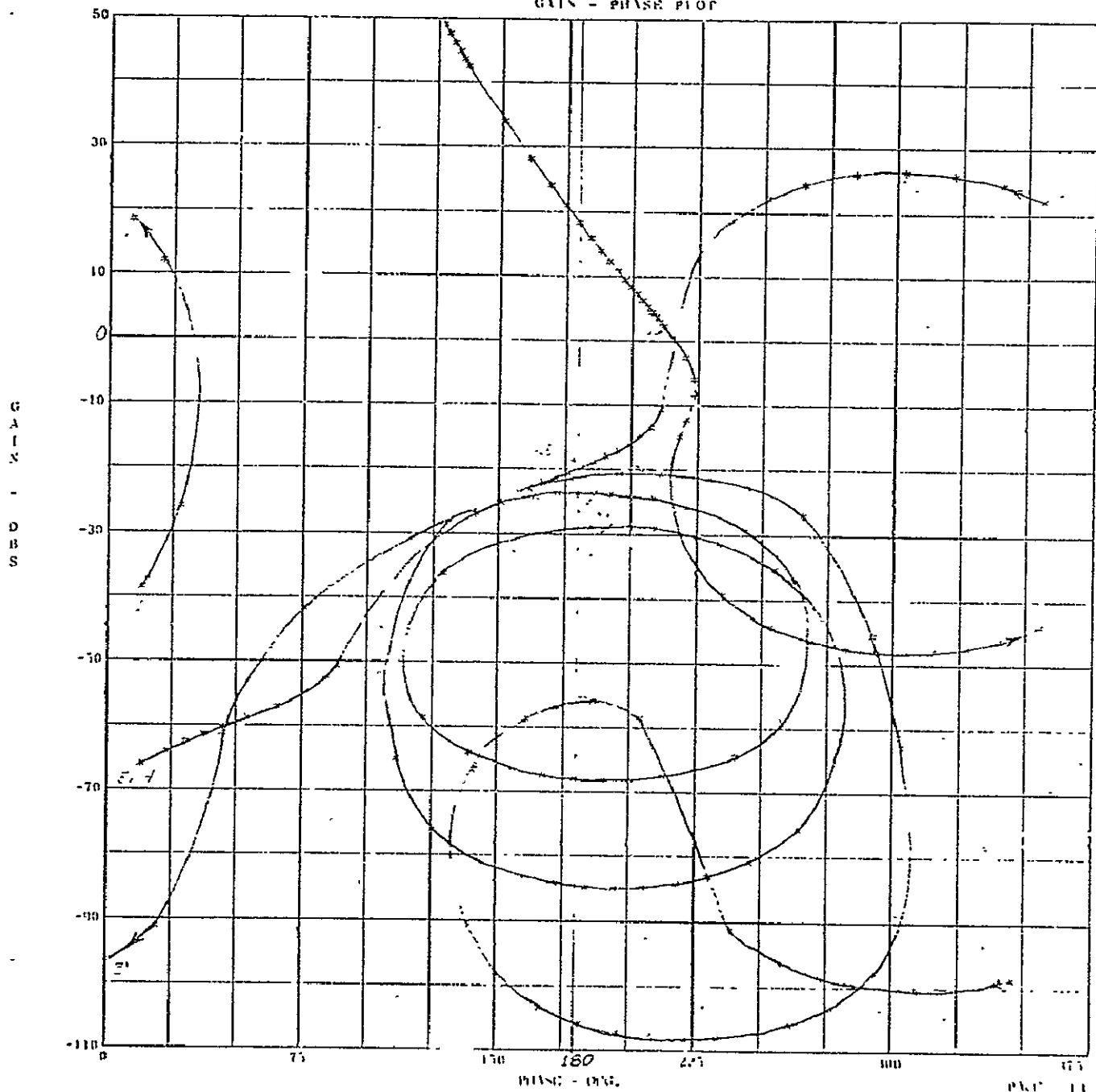


Figure 45
S-PLANE FREQUENCY RESPONSE OF THE
COMPENSATED SYSTEM USING THE SCS